Physics – Uspekhi **37** (10) 937 – 961 (1994) ©1994 Jointly Uspekhi Fizicheskikh Nauk and Turpion Ltd

REVIEWS OF TOPICAL PROBLEMS PACS numbers: 29.27.Ac; 29.27.Eg; 61.80.Mk

Steering of high-energy charged-particle beams by bent single crystals

V M Biryukov, V I Kotov, Yu A Chesnokov

Contents

Abstract. A review is given of the results of investigations of the channelling of high-energy charged particles in bent single crystals carried out in the last fifteen years. These investigations have given rise to new applications of crystals in the control of high-energy particle beams in modern accelerators: in beam lines, in systems for the extraction of accelerated beams, and in certain experiments.

1. Introduction

Interest in the passage of charged particles through crystals first appeared at the beginning of the century following experiments on x-ray diffraction in crystal lattices, which provided the proof of an ordered distribution of atoms in a crystal. Stark put forward the hypothesis [1] that certain directions in a crystal should be relatively transparent to charged particles. He proposed to check this hypothesis in experiments on proton beams.

These first ideas on the channelling of charged particles in crystals had been forgotten and became topical again in the early sixties when the channelling effect was rediscovered by computer simulation [2] and in experiments [3] which revealed anomalously long ion ranges in crystals. The orientational effects during the passage of charged particles through crystals have been found for a whole range of processes characterised by small impact parameters of collisions between particles and atoms: nuclear reactions, large-angle scattering, energy losses. Lindhard explained the channelling of charged particles in crystals [4]. The results of numerous investigations of the channelling of low-energy (amounting to several megaelectron-volts) charged particles in crystals have been summarised in several monographs and reviews [5 – 8].

A new stage in the investigation of the channelling of charged particles is the extension to high energies. These investigations have been stimulated by the idea of E N Tsyganov (1976) who demonstrated theoretically that it should be possible to steer high-energy charged particles by bent crystals. His idea was confirmed in pioneering experiments carried out in 1979 in collaboration between the Joint Institute of Nuclear Research (JINR) in Dubna and the Fermi National Accelerator Laboratory (FNAL) in Batavia, IL. In the first experiments on bent crystals the efficiency of the particle beam deflection (i.e. the ratio of the intensity of the deflected beam to that incident on a crystal) was very low (a fraction of 1%), but in the subsequent experiments it has been improved to 10% and has recently reached a record value of ~50% in experiments on deflection of a 450 GeV proton beam at CERN in Geneva.

Experiments carried out in 1990 on the accelerator at our Institute of High-Energy Physics (IHEP) in Protvino, in collaboration with the Leningrad Institute of Nuclear Physics (LINP) in Gatchina, demonstrated that it is

V M Biryukov, V I Kotov, Yu A Chesnokov Institute of High-Energy Physics, 142284 Protvino, Moscow Region. Tel. (095) 217 49 53

Received 12 May 1994
Uspekhi Fizicheskikh Nauk **164** (10) 1017 – 1040 (1994)
Translated by A Tybulewicz

possible not only to deflect charged particle beams in a bent crystal but also to focus them in the bending plane. This can be achieved if the exit face of a crystal is shaped to form a cylindrical surface, so that all the planes tangential to the atomic planes in the exit face of a crystal intersect at some distance from the crystal. Bent crystals with their extremely high interplanar electric fields (10^9 V cm^{-1} or higher) can thus be used to control beams of charged particles with high and very high energies. This possibility has been realised by many leading research centres working on high-energy physics. Studies are being made of the use of bent crystals for the extraction of accelerated proton beams, in beam lines, and in certain experiments. In all three cases some interesting and very promising results have been obtained. In particular, bent crystals have been used to extract accelerated protons with energies up to 8 GeV at JINR (1984), up to 70 GeV at IHEP (1989), and 120 GeV at CERN (1993). In the JINR experiment the extraction efficiency was 10^{-4}, but it has been improved to 3×10^{-3} at IHEP and to 10^{-1} at CERN. The experiments proceeding at CERN and planned at FNAL are designed to achieve highly efficient extraction of a proton beam, so that the results can then be used to develop an extraction system for supercolliders of the large hadron collider (LHC) type, because the use of crystals for this purpose seems to be the only method which can ensure that experiments can be carried out in the collider mode and with a fixed target.

In this review we shall confine ourselves to the presentation of the results of the experiments carried out in the last fifteen years and representing the development of new applications of crystals in control of beams of high-energy particles.

2. Channelling of charged particles in crystals

2.1 Equations of motion

Lindhard [4] demonstrated that for a low angle of incidence of a charged particle, relative to a crystallographic axis or plane, the successive collisions of the particle with the lattice atoms are correlated with one another and it is necessary to consider the interaction of a charged particle with an atomic string or plane. In the low-angle approximation the potentials of the individual atoms can be replaced with an average continuous potential. If a particle is not oriented exactly along an atomic string but moves at a small angle relative to a crystallographic plane, it is possible to use the continuous potential of an atomic plane where the averaging is carried out over two coordinates:

$$U_{\mathrm{pl}}(x) = Nd_{\mathrm{p}} \int_{-\infty}^{+\infty} \int_{-\infty}^{+\infty} V(x,y,z)\,\mathrm{d}y\,\mathrm{d}z\,, \qquad (1)$$

where $V(x,y,z)$ is the potential of the interaction of the particle with an atom; N is the number of atoms per unit volume; d_{p} is the distance between the adjacent planes. The motion of heavy particles (protons, ions) can be considered in terms of classical mechanics and the precision of this approximation improves as the energy of the particle increases [4]. In the case of light particles (electrons, positrons) the classical approximation becomes valid in the megaelectron-volt range of energies. Since we shall consider planar channelling, we shall give the potential of Eqn (1) describing the interaction between a particle with a charge $Z_i e$ and an atomic plane of a crystal with an atomic number Z on the basis of the Moliere approximation

$$U_{\mathrm{pl}}(x) = 2\pi N d_{\mathrm{p}} Z_i Z e^2 a_{\mathrm{TF}} \sum_{i=1}^{3} \frac{\alpha_i}{\beta_i} \exp\left(-\frac{\beta_i x}{a_{\mathrm{TF}}}\right)\,. \qquad (2)$$

Here $\alpha = 0.1$, 0.55, and 0.35 and the corresponding values of β are 6.0, 1.2, and 0.3; the Thomas–Fermi screening parameter is $a_{\mathrm{TF}} = 0.8853 a_{\mathrm{B}} Z^{-1/3}$, where $a_{\mathrm{B}} = 0.529$ Å. Another frequently used approximation is due to Lindhard:

$$U_{\mathrm{pl}}(x) = 2\pi N d_{\mathrm{p}} Z_i Z e^2 \left(\sqrt{x^2 + 3a_{\mathrm{TF}}^2} - x\right)\,. \qquad (3)$$

The thermal vibrations of atoms alter the potential of the static lattice of Eqn (1) near a plane at distances of the order of the amplitude u of these vibrations; the modified potential is discussed in Ref. [5]. A particle moving in a crystal is in a potential which is the sum of the potentials of the individual planes. Examples of the potentials of the (110) and (111) planes of silicon are given in Fig. 1. The depth of the potential well U_0 in silicon is of the order of 20 eV.

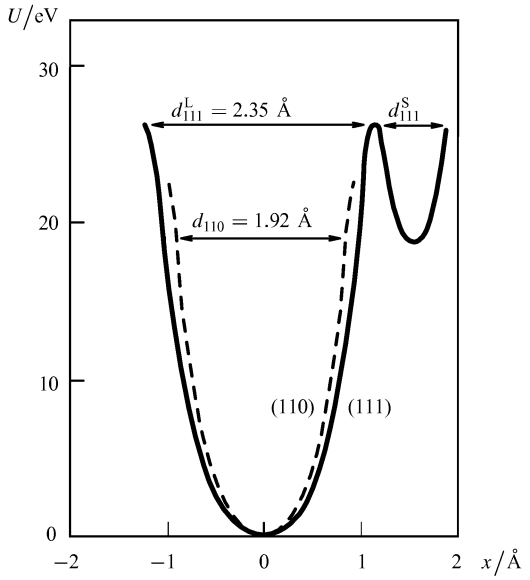

Figure 1. Calculated continuous potentials in the (110) and (111) planes of silicon.

The transverse motion of a particle arriving at a small angle (a typical range of these angles will be given below) relative to any of the crystallographic axes or planes is governed by the continuous potential of the crystal lattice. It is clear from the above discussion that the fields of atomic strings and planes form potential wells in which the motion of particles can be stable. In this case one speaks of the *channelling* of a particle: it is axial channelling if the particle is coupled to atomic strings and planar channelling if the particle is coupled to atomic planes.

The interaction of a channelled particle with a crystalline medium differs strongly from the interaction with an amorphous body or a misoriented crystal. A channelling proton does not in fact collide with nuclei. Moreover, it moves in a medium that has a reduced electron density.

Such a proton is very sensitive to crystal lattice defects and this has provided a basis for an effective method for the analysis of crystal quality [7]. In the case of light particles the coherent effects are also demonstrated by an increase in the probability of the emission of a photon or creation of a pair, and by interesting spectra [9–13]. A channelling particle may travel a distance of a few centimetres in a crystal (when its energy is in the gigaelectron-volt range).

Let us now consider the equations of motion of a particle with a high energy $(p^2c^2 + m^2c^4)^{1/2}$ in a transverse potential $U(x)$. If the transverse component p_x of the momentum p of this particle is much less than the longitudinal component p_z (i.e. if the angle $\theta = p_x/p_z$ is small), we can write down the equation of conservation of the total energy $E = (p_x^2c^2 + p_z^2c^2 + m^2c^4)^{1/2} + U(x) = \text{const}$ in the form

$$\frac{p_x^2c^2}{2E_z} + U(x) + E_z = \text{const} \ . \tag{4}$$

where $E_z = (p_z^2c^2 + m^2c^4)^{1/2}$. The sum of the first two terms in Eqn (4), which depends on the transverse momentum and the transverse coordinate, is called the transverse energy E_x. The longitudinal component of the momentum is conserved during motion in the potential $U(x)$, which implies conservation of E_x:

$$E_x = \frac{p_x^2c^2}{2E_z} + U(x) = \frac{p_z^2c^2}{2E_z}\theta^2 + U(x) = \text{const} \ . \tag{5}$$

If we assume that $E_z \approx E$ and $p_z \approx p$, and if we apply the familiar relationship $pc^2 = vE$, where v is the particle velocity, Eqn (5) can be rewritten in the form

$$E_x = \frac{pv}{2}\theta^2 + U(x) = \text{const} \ .$$

Differentiation of Eqn (5) with respect to z and the substitution of the same quantities as before gives

$$pv\frac{\mathrm{d}^2x}{\mathrm{d}z^2} + U'(x) = 0 \tag{6}$$

for one-dimensional tranverse motion in the potential $U(x)$. It describes oscillations of a particle in the potential well of a planar channel. In the harmonic potential $U_0(2x/d_p)^2$ the period λ of these oscillations is equal to $\pi d_p(pv/2U_0)^{1/2}$. The period λ is macroscopic: its value is up to 0.5 mm for a 20 TeV proton in silicon. The condition for the capture of a particle into the channelling mode is

$$\frac{pv}{2}\theta^2 + U(x) < U_0 \ . \tag{7}$$

Hence, if $x = 0$, the limiting angle of capture (channelling angle) is

$$\theta_L = \left(\frac{2U_0}{pv}\right)^{1/2} \ . \tag{8}$$

The angles θ_L for planar and axial channelling were introduced by Lindhard. For the (110) planes in silicon the angle θ_L is 20 μrad if the particle energy is 100 GeV and is 7 μrad for 1 TeV. The scattering by nuclei rapidly destroys the channelled motion: a particle approaching an atomic plane to a distance of the order of a_{TF} can be regarded as dechannelled. For a channelled particle the critical transverse coordinate is $x_c \approx (d_p/2) - a_{TF}$ and the critical channelling angle is $\theta_c = (2E_c/pv)^{1/2}$, where $E_c = U(x_c)$ is the critical transverse energy. The definition of x_c may include the dependence on the thermal vibrations of atoms. The experiments at FNAL [14] have shown that an accurate estimate of the 'half-thickness' of an atomic plane or layer is $2.5u$.

A phase diagram in the (x, θ) plane provides a convenient illustration of the capture of a particle into the channelling mode (Fig. 2). Fig. 2 shows the distribution of 450 GeV protons in silicon with the (111) orientation, obtained by computer simulation [54]. The elliptic patterns represent the phase paths described by Eqn (5) and correspond to different values of E_x. The outer ellipse corresponds to the critical transverse energy E_c. The phase region inside this ellipse is occupied by channelled particles. The particles outside the ellipse are not channelled.

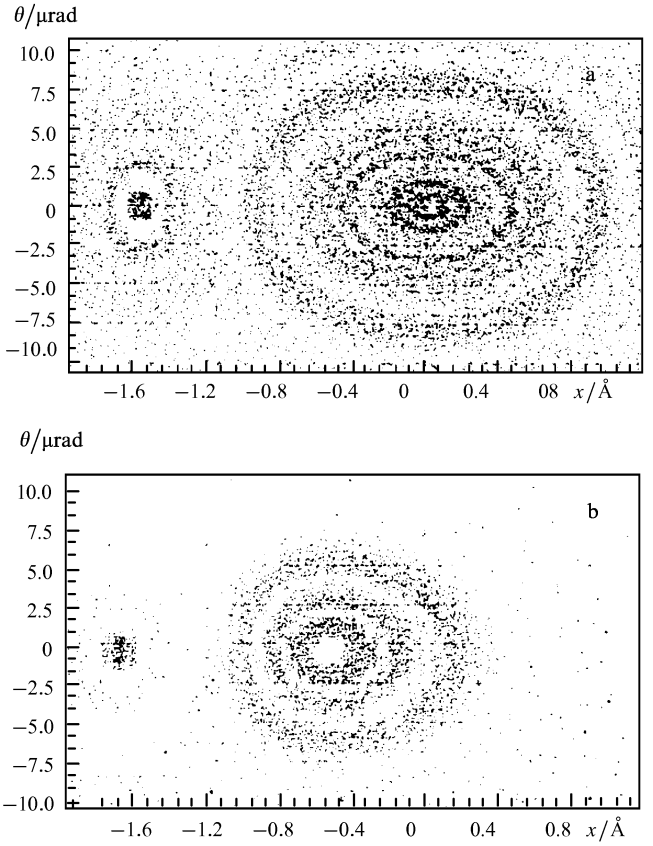

Figure 2. Distribution of 450 GeV protons in (111) silicon, plotted in the (x, θ) plane on the basis of a computer simulation [54]: (a) straight crystal; (b) bent crystal ($pv/R = 1.5$ GeV cm^{-1}).

At the entry to a crystal the particles are distributed uniformly along x between $-d_p/2$ and $d_p/2$. If their angular distribution between $-\theta_c$ and θ_c is also uniform, which is typical of gigaelectron-volt beams, the probability of the capture of a particle into the channelling mode is the ratio of the area of the phase ellipse $E_x = E_c$ (i.e. the planar channel acceptance) to the area of the whole phase region occupied by the incident beam (its emittance). In the case of the harmonic interplanar potential and a straight crystal this probability is

$$A_s = \frac{2x_c}{d_p}\frac{\pi}{4}\frac{\theta_c}{\Phi} \tag{9}$$

if the beam divergence is 2Φ. If a particle is incident exactly parallel to the crystallographic planes, the probability of its capture into the channelling mode is simply $2x_c/d_p$. When it is incident at a fixed angle θ, then in the harmonic approximation this probability decreases by the factor $[1-(\theta^2/\theta_c^2)]^{1/2}$.

2.2 Channelling in a bent crystal

One can expect particles travelling in a slightly bent single crystal to follow the directions of the bent planes or axes and thus become deflected from the initial direction by the bending angle of the crystal. The possibility of this effect was pointed out and the suggestion to use it in the control of high-energy particle beams was made by Tsyganov in 1976 [15] and realised experimentally [16] at JINR in 1979. Let us consider the channelling of a charged particle in a planar channel with a constant bending radius R. If the particle is described by the local coordinates x and θ relative to the atomic planes at a point z, we can use Eqn (6) and supplement it by the centrifugal force pv/R:

$$pv\frac{d^2x}{dz^2}+U'(x)+\frac{pv}{R}=0\ . \tag{10}$$

The particle then moves as if it were in an effective interplanar potential

$$U_{\rm eff}(x)=U(x)+\frac{pv}{R}x\ .$$

Examples of the potentials $U(x)$ and $U_{\rm eff}(x)$ are shown in Fig. 3 for the (110) planes in silicon. It is obvious that an increase in the curvature pv/R reduces the depth of the effective potential well and at some critical value $(pv/R)_c$ this well disappears and the channelling becomes impossible. The critical bending angle is governed by the maximum interplanar field $(pv/R)_c=U'_{\max}$. This quantity is about 6, 12, and 48 GeV cm^{-1} for the (110) planes in silicon, germanium, and tungsten, respectively. Usually, the maximum of $U'(x)$ is reached near an atomic plane where the nuclear scattering is strong so that the critical radius R_c is determined more by the derivative of the potential at the boundary of a channel: $R_c=pv/U'(x_c)$. For silicon, we have $U'(x_c)\approx 5$ GeV cm^{-1}.

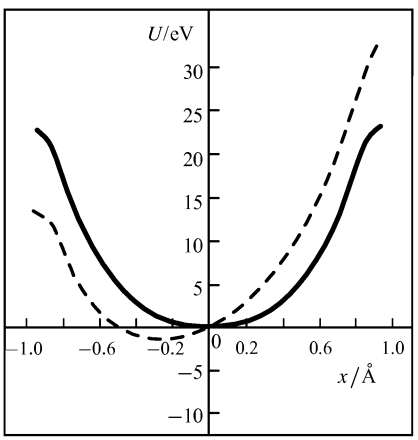

Figure 3. Examples of the potentials $U(x)$ (continuous curve) and $U_{\rm eff}(x)$ (dashed curve) for the (110) plane of silicon.

The phase region where the particle channelling occurs in a bent silicon crystal with the (111) orientation is identified in Fig. 2b. On increase in the crystal bending pv/R the size of this region decreases and it shifts closer to an atomic plane. This is accompanied by a corresponding reduction in the acceptance A of a planar channel [31–33]. In the harmonic approximation for $U(x)$ this dependence is of elementary nature. The effective potential remains harmonic, so that the particles still execute sinusoidal oscillations (with a period independent of R) but there is a new equilibrium position $x_0=x_cR_c/R$. The depth of the well E_c decreases by the factor $[1-(R_c/R)]^2$. For the particles incident parallel to atomic planes only the reduction in the range of x available for channelling is important: this range is $-x_c+2x_0<x<x_c$. The acceptance is then [33]

$$A=\frac{2x_c}{d_p}\left(1-\frac{R_c}{R}\right)\ , \tag{11}$$

where $2x_c/d_p$ is the acceptance of a straight channel. For a beam with a uniform angular distribution and a half-width $\Phi>\theta_c$, the acceptance A is represented by the ratio of the area of the phase region available for channelling to the beam emittance, i.e.

$$A=\frac{2x_c}{d_p}\frac{\pi}{4}\frac{\theta_c}{\Phi}\left(1-\frac{R_c}{R}\right)^2\ . \tag{12}$$

The acceptance decreases by the following factor, compared with that applicable to a straight crystal (9):

$$A_b\approx\left(1-\frac{R_c}{R}\right)^2\ .$$

Fig. 4 shows the function $1-A_b(pv/R)$, calculated in the Moliere approximation for the (110) channel in silicon at two temperatures of 293 K and 128 K (on the assumption that $x_c=d_p-2.5u$). This figure includes also the experimental results obtained at FNAL [14]. It is evident from the figure that the acceptance decreases strongly well before the critical bending is reached. In the case of a silicon

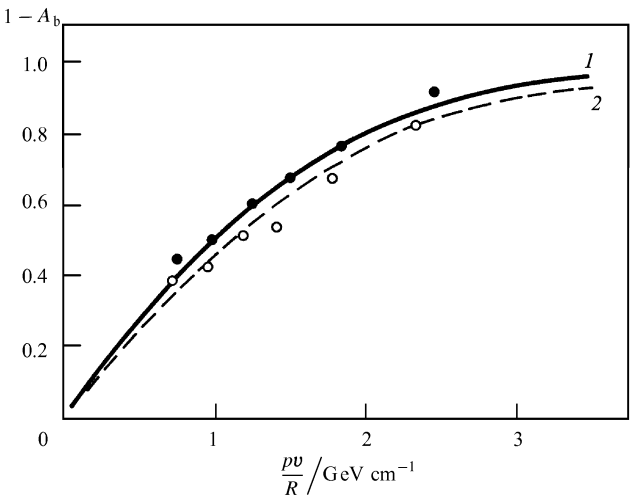

Figure 4. Functions $1-A_b(pv/R)$ for Si(110) at two temperatures: (*1*) 293 K; (*2*) 128 K [14]. The experimental points were obtained at the Fermi National Accelerator Laboratory and the calculations were made in the Moliere approximation ($x_c=d_p-2.5u$).

deflector the threshold value is approximately 1 GeV cm^{-1} and for germanium it is about 2 GeV cm^{-1}.

Experiments on proton beam deflection in silicon and germanium single crytals have been carried out in the energy range from 1 to 800 GeV at LINP [19], JINR [16, 17], IHEP [18, 24, 39, 47, 48, 84], CERN [20, 25, 55, 56, 59], and FNAL [14, 21, 45]. Also beams of electrons [22] and heavy nuclei [23] have been deflected. The maximum angle of proton deflection has reached 130 mrad [84] and the maximum intensity attained is 10^{10} protons per cycle [24]. The bending efficiency has reached 50% of the whole beam incident on a crystal [25]. Experiments have revealed that channelling occurs in a silicon crystal with a curvature pv/R up to 3–4 GeV cm^{-1}, i.e. close to the critical value.

2.3 Dechannelling in a straight crystal

The scattering of a channelled particle on electrons and nuclei (and on the lattice defects) results in nonconservation of E_x. The scattering alters the state of the particle which may leave the channelling mode (*dechannelling* process). The reverse transitions are also possible: from the unchannelled fraction of the beam to the channelling mode (*rechannelling* or *volume capture*). These processes can be described by transport equations [8, 34] or by computer simulation [54, 58]. The following one-dimensional diffusion equation for the particle distribution function $f(E_x, z)$ is used most frequently in the description of dechannelling:

$$\frac{\partial f}{\partial z} = \frac{1}{2}\frac{\partial}{\partial E_x}\left[D(E_x)\frac{\partial f}{\partial E_x}\right] , \tag{13}$$

where $D(E_x)$ is the diffusion coefficient. The use of Eqn (13) makes it possible to provide a simple analytic interpretation of the dechannelling process. The linear approximation $D \approx D_0 E_x$ describes well the channelled particles [8]. In this case the distribution function is [36, 37]

$$f = \sum_{k=1}^{\infty} C_k J_0\left(j_{0,k}\sqrt{\frac{E_x}{E_c}}\right)\exp\left(-\frac{D_0 j_{0,k}^2 z}{4E_c}\right) , \tag{14}$$

where C_k is governed by the initial particle distribution f_0:

$$C_k = \frac{1}{E_c J_1^2(j_{0,k})}\int_0^{E_c} f_0(E_x) J_0\left(j_{0,k}\sqrt{\frac{E_x}{E_c}}\right) \mathrm{d}E_x . \tag{15}$$

Here, $j_{0,k}$ is the kth zero of the Bessel function J_0. We can see from the distribution function (14) that the rate at which the $k > 1$ terms of the series decrease is in accordance with $j_{0,k}^2 \propto k^2$. After an initial section the terms with $k > 1$ become smaller and the particle distribution is then described by the first term of the expansion of the function (14):

$$f = C_1 J_0\left(j_{0,1}\sqrt{\frac{E_x}{E_c}}\right)\exp\left(-\frac{D_0 j_{0,1}^2 z}{4E_c}\right) . \tag{16}$$

Therefore, in the interior of a crystal the fraction of the channelled particles falls exponentially, proportionally to $\exp(-z/L_D)$,and the process is characterised by the *dechannelling length*

$$L_D = \frac{4E_c}{j_{0,1}^2 D_0} , \tag{17}$$

which no longer depends on the initial particle distribution.

The relaxation length L_{rel} for the distribution function (16) is governed primarily by the rate of fall of the second term in the function (14) and this length is of the order of

$$L_{rel} \approx \left(\frac{j_{0,1}}{j_{0,2}}\right)^2 L_D \approx 0.2 L_D . \tag{18}$$

If the length of a crystal is less than this characteristic quantity, then the experimentally determined dechannelling length depends on the initial parameters of a particle beam incident on a crystal: for example, it may depend on the nature of capture (end face or volume) or on the beam divergence (small, of the order of θ_c, or much greater).

The quantity D_0 (friction coefficient) is governed by the mean-square value of the angle of scattering on electrons and nuclei:

$$D_0 = \frac{pv}{2}\left\langle\frac{(\delta\theta_s)^2}{\delta z}\right\rangle . \tag{19}$$

In view of the discrete nature of the crystal lattice, the contribution of fluctuations of the potential to the pure planar channelling is much less than the contribution of multiple scattering on nuclei [8]. If we set the limits by $x_c \leqslant (d_p/2) - a_{TF}$, we need to consider only the scattering on electrons. According to Lindhard [4],

$$\left\langle\frac{(\delta\theta_s)^2}{\delta z}\right\rangle = \frac{m_e}{2p^2}\left(\frac{\delta E}{\delta z}\right)_{am}\frac{n_e(x)}{n_{am}} . \tag{20}$$

Here, $n_e(x)$ is the electron density considered as a function of the coordinate; n_{am} is the average (amorphous) electron density; m_e is the rest mass of an electron. Averaging of $n_e(x)$ over the range $|x| < x_c$ gives the dechannelling length (17):

$$L_D = \frac{16}{j_{0,1}^2}\frac{pv}{Z_i L_e r_e m_e c^2}\frac{U(x_c)x_c}{(\partial U/\partial x)_{x=x_c}} . \tag{21}$$

Here, r_e is the classical radius of an electron and L_e is the Coulomb logarithm [38]; for details see the derivation in Ref. [39]. The second factor in the expression (21) contains the energy dependence and the third factor represents the dependence on the properties of matter. Substituting $j_{0,1} \approx 3\pi/4$ and applying the Lindhard potential (3) we can rewrite expression (21) in its final form (for $\gamma \gg 1$):

$$L_D = \frac{256}{9\pi^2}\frac{pv}{\ln(2m_e c^2\gamma/I) - 1}\frac{a_{TF}d_p}{Z_i r_e m_e c^2} , \tag{22}$$

where I is the ionisation potential (172 eV for silicon). It is evident from expression (22) that the dechannelling length is proportional to d_p. The temperature dependence is ignored here and the substitution $x_c \approx d_p/2$ is made. If the dependence $x_c(u)$ is introduced, then L_D decreases with rising temperature [40]. A silicon crystal with the (110) orientation represents a regular structure with the same distance $d_p = 1.92$ Å between the planes. In a crystal with the (111) orientation a large interplanar distance $d_p^L = 2.35$ Å alternates periodically with a smaller distance d_p^S (Fig. 1), where $d_p^S \approx d_p^L/3$. In the case of long (111) silicon crystals we can ignore the particles that move inside the small interplanar gap d_p^S.

The dependences (22) calculated for the (110) and (111) channels in silicon are plotted in Fig. 5 together with the experimental data obtained at JINR, CERN, IHEP, and

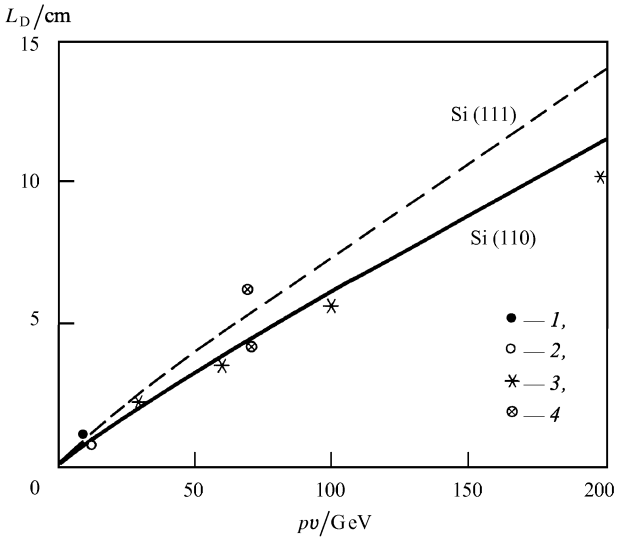

Figure 5. Calculated dependences $L_D(pv)$ plotted for the Si(110) and Si(111) channels alongside the experimental data: (*1*) JINR [16]; (*2*) CERN [20]; (*3*) FNAL [21]; (*4*) IHEP [39].

FNAL. For $E = 70$ GeV a calculation based on expression (22) gives $L_D^{(111)} = 5.4$ cm for (111) silicon crystals and $L_D^{(110)} = 4.4$ cm for (110) silicon, in satisfactory agreement with the experiments. A logarithmic correction to the linear extrapolation $L_D \propto pv$ amounts to tens of percent in the experimentally investigated range of energies. The dependence on the properties of matter reduces to the factor $a_{TF} d_p$; this leads to the dependence $L_D \propto Z^{-1/3}$ for isomorphous ($d_p = \text{const}$) lattices (for example, Si and Ge). The ratio $L_D^{(111)}/L_D^{(110)}$, estimated on the basis of expression (22), should be of the order of $d_p^{(111)}/d_p^{(110)} = 1.23$ for silicon. The experimental ratio is 1.4 ± 0.2.

We have considered so far the dechannelling in crystals with an ideal lattice. Real crystals contain defects. Of all the possible lattice defects—point (interstitial atoms and vacancies), linear (dislocations), two-dimensional (stacking faults), and three-dimensional (amorphous clusters)— those of the greatest interest are dislocations because the dechannelling due to other defects becomes weaker or remains constant when energy is increased [7]. Dislocations induce local lattice distortions. Therefore, a channelled particle may reach a region with a strong curvature of the channel; alternatively it may be scattered by nuclei or perturbations of the lattice potential. Thus, the lattice perturbation in the vicinity of a linear dislocation alters the local channel curvature $1/R_{loc}$ by an amount of the order of b/r^2, where r is the distance to the dislocation and b is the Burgers vector. This curvature exceeds the critical value $1/R_c$ at distances up to $r_D \approx (bR_c)^{1/2}$ from a dislocation [61]. We can arbitrarily asume that a particle becomes dechannelled if it enters a cylinder with a diameter $\sigma_D \approx 2r_D$ around a dislocation. The dechannelling length $L_D = 1/n_D\sigma_D$ depends on the dislocation density n_D and decreases as $(pv)^{-1/2}$ when the particle energy is increased. At currently attainable energies (hundreds of gigaelectronvolts) and for the high-quality silicon crystals now available, the defects do not influence the beam deflection efficiency. The contribution of different types of dislocation defects to the dechannelling in the teraelectron-volt energy range is discussed in Ref. [60]. Experimental estimates can be found in Section 3.2.1 below.

2.4 Dechannelling in a bent crystal

Bending of a crystal displaces the channelled particles closer to an atomic plane so that the diffusion coefficient of the particles differs from the value for a straight crystal. The valence electrons in silicon and germanium are distributed approximately uniformly in a channel so that the diffusion coefficient $D(E_x)$ is insensitive to weak bending [41, 42]. The E_x diffusion increases in a strongly bent crystal.

Channelling is influenced mainly by a bending-induced reduction of the phase volume in which the channelling takes place. Relationship (17) links the dechannelling length L_D to the critical transverse energy E_c, which depends strongly on the channel curvature: $L_D \propto E_c(pv/R)$ [42]. Since for the harmonic potential the value of $E_c(pv/R)$ is $E_c(0)[1 - (R_c/R)]^2$, it follows that the dechannelling length can be written as:

$$L_D(p, R) = spv\left(1 - \frac{R_c}{R}\right)^2 , \tag{23}$$

where spv is the dechannelling length in a straight crystal given by expression (22). In the harmonic approximation the dependence of L_D on p is, for a given radius R,

$$L_D(p) = spv\left(1 - \frac{p}{p_c}\right)^2 . \tag{24}$$

The quantity L_D vanishes at $pv = (pv)_c = RU'(x_c)$. The maximum of L_D corresponds to $p = p_c/3$.

Forster et al. [14] measured L_D of protons in the range of p from 60 to 200 GeV/c for a (110) silicon crystal bent to a radius of about 80 cm; this was done at two temperatures: room and 128 K. Solid-state detectors selected particles with low dE/dz losses in the part of a crystal near the entry (this is a widely used criterion in selection of the channelled particles). The angular distribution of these particles behind the crystal was nearly exponential. The dependence $L_D(p)$

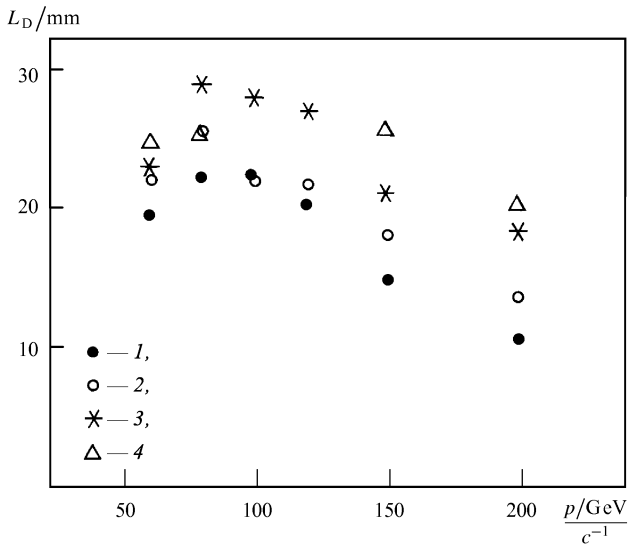

Figure 6. Dechannelling length, plotted as a function of the momentum for a bent Si(110) crystal at two temperatures: (*1, 2*) 293 K; (*3, 4*) 128 K. (*1, 3*) Experimental results from Ref. [14]; (*2, 4*) CATCH computer simulation.

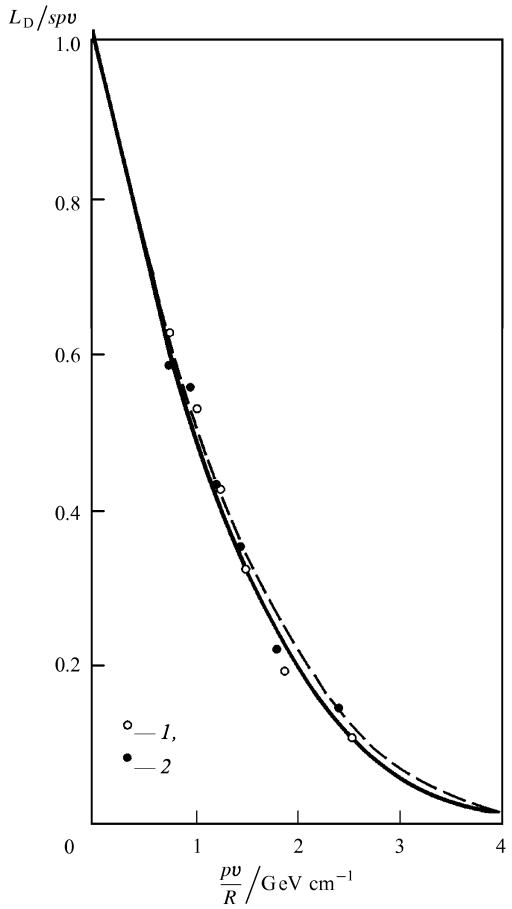

Figure 7. Ratio of the dechannelling length for bent and straight silicon crystals. The curves represent a computer simulation of the dependence $L_D/spv = E_c(pv/R)/E_c(0)$. The points are the experimental results taken from Ref. [14]; the best value of s is found by fitting [43]. The continuous line and the open circles (*1*) correspond to room temperature and $s = 0.54$ mm GeV^{-1}. The dashed curve and the black dots (*2*) correspond to 128 K and $s = 0.65$ mm GeV^{-1}.

obeyed expression (24) (Fig. 6). The experimental results are compared in Fig. 7 with the model described by the expression

$$L_D = spv\frac{E_c(pv/R)}{E_c(0)} ;$$

the value of s was selected by fitting to the Moliere potential. It is evident from Fig. 7 that the model describes well the dependence of L_D on pv/R. The values $s = 0.54$ mm GeV^{-1} at room temperature and $s = 0.65$ mm GeV^{-1} at 128 K obtained by fitting are also in excellent agreement with the calculations based on the expression (22), which yields $s = 0.62$ mm GeV^{-1}, as well as with the experimental data on straight crystals ($s = 0.59$ mm GeV^{-1} at room temperature [39]) obtained in this energy range. The influence of temperature, which is weak for a straight crystal, becomes greater for a bent crystal as pv/R increases, which is to be expected on the basis of the diffusion model [40].

2.4.1 Efficiency of beam deflection by a crystal

The number of particles A_s captured into the channelling mode on the face of a crystal is governed primarily by the divergence of the incident beam, as described by expression (9). It follows from general equations (10) and (14) that the fraction of the particles deflected by a crystal through the bending angle Θ, i.e. the efficiency F of a crystal, depends only on two variables pv/R and Θ (and on the properties of the crystal). This means that for any bending angle Θ we can select the optimal curvature $(pv/R)_{opt}$ for which $F(pv/R, \Theta)$ is maximal. The efficiency of a perfect crystal thus depends only on the angle Θ and on the properties of this crystal, but not on the particle energy.

We shall illustrate this explicitly in the harmonic approximation. If a crystal is sufficiently long (when the length L is of the order of L_D), the dechannelling losses can be taken into account by the exponential factor $\exp(-L/L_D)$. We can then estimate F if we combine Eqns (12) and (23) [42, 44]:

$$F = A_s\left(1 - \frac{R_c}{R}\right)^2 \exp\left\{-\frac{R}{R_c}\frac{\Theta}{\Theta_D[1 - (R_c/R)]^2}\right\} . \quad (25)$$

We have introduced above a constant $\Theta_D = spv/R_c$, which represents the ratio of the dechannelling length spv in a straight crystal to the critical radius R_c; Θ_D depends only on the properties of a crystal and amounts to ~ 0.3 rad for Si(110). The expression for the efficiency (25) is universal. The properties of a crystal affect only Θ_D and A_s. Fig. 8

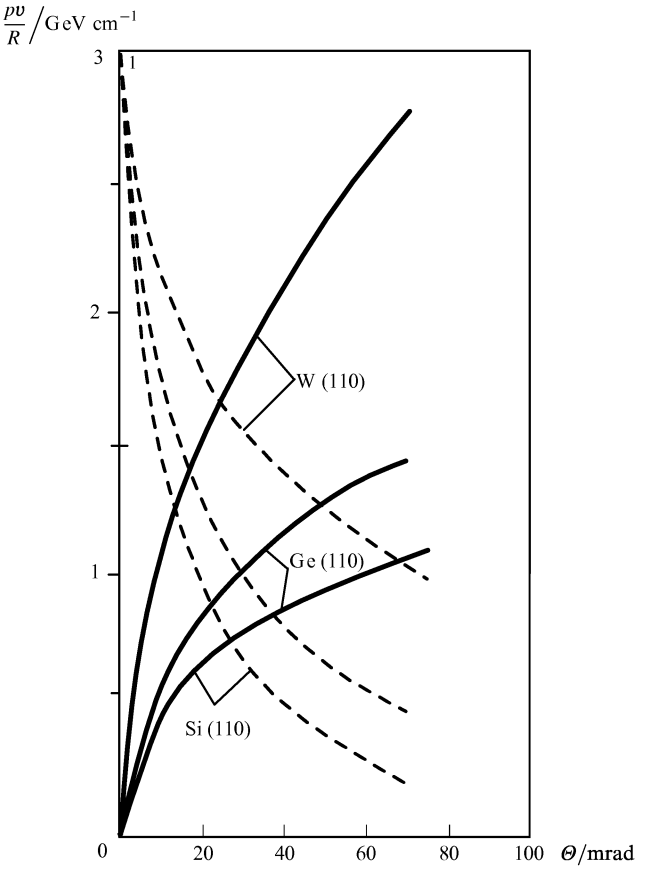

Figure 8. Results of optimisation of the deflection efficiency on the basis of the Moliere potential [43]. The continuous curves represent the optimal curvature pv/R and the dashed curves give the corresponding limiting efficiecy F/A_s as a function of Θ for Si(110), Ge(110), and W(110) deflectors.

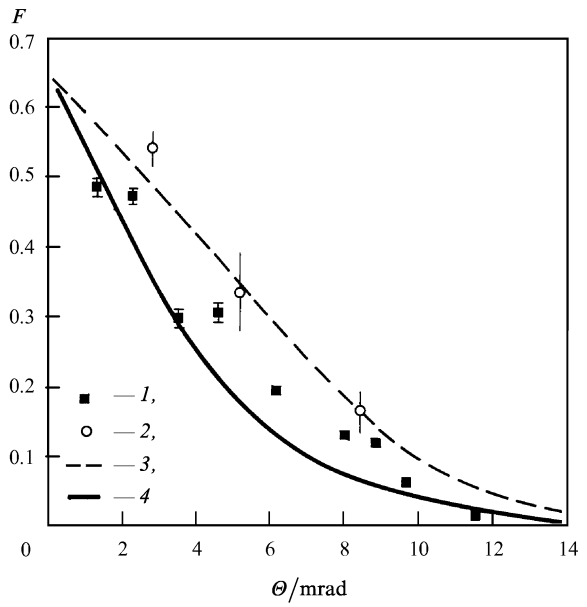

Figure 9. Measured efficiency of deflection of a 450 GeV proton beam by bent crystals: (*1*) Si(111) [53]; (*2*) Si(110) [59]. The curves are calculated for uniform bending of a crystal (*3*) and three-point bending (*4*) [53].

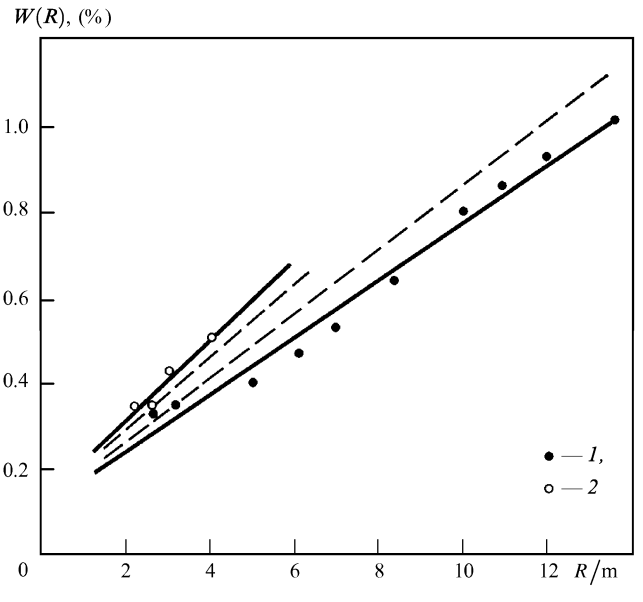

Figure 10. Probability of volume capture of 70 GeV protons plotted as a function of the radius of curvature of an Si(111) crystal [48] in the case of rising (*1*) and falling (*2*) curvatures. The dashed lines are the values corrected for the gradient [expression (28)].

shows the results of optimisation carried out using the Moliere potential [43]: the optimal curvature pv/R and the corresponding efficiency limit are plotted as a function of Θ for Si(110), Ge(110), and W(110) deflectors.

In the experiments the efficiency is limited usually by the smallness of the ratio $\theta_c/\Phi \ll 1$. This difficulty has been avoided in the work carried out at CERN [53, 55, 56, 59] on a beam of 450 GeV protons with a small (± 3 μrad) divergence, which should be compared with $\theta_c \approx 9$ μrad for Si(111). When an Si(111) crystal was inserted in this beam, the width of the orientational dependence of the intensity of the deflected beam was only 17 μrad $\approx 2\theta_c$ [53]. The measured efficiency of proton deflection by silicon crystals with the (111) [53] and (110) [59] orientations is plotted in Fig. 9. The efficiency achieved was ≈50% for angles of ∼2 mrad. The experimental results were in excellent agreement with the calculations [53] based on the model of Refs [32] and [44] (see Fig. 9).

2.5 Volume capture

The particles unchannelled at the front of a crystal may be captured into the channelling mode in its interior (*volume capture or feeding-in*) as a result of scattering or a change in the curvature of a crystal. Such transitions to channelling are interesting as a means of extending the capabilities of crystal optics of charged beams. The dechannelling reversibility follows from the Lindhard reversibility rule [4], according to which the probability of the scattering of a particle from a specific channelled state to a specific unchannelled state is equal to the probability of the reverse process.

This rule has been demonstrated in experiments on gigaelectron-volt beams [19, 45] in which dE/dz (energy-loss) solid-state detectors, distributed over the length of a crystal, have been used to find the state of each particle. The volume capture of particles, due to multiple scattering, has been observed for the first time experimentally for beams of ions of ∼1 MeV energy [46]. Effective dechannelling of a beam in a crystal also depends on the processes of particle exchange between the channelled and unchannelled fractions of the beam. In particular, a dynamic equilibrium may be established between the fractions if there is no effective dechannelling [47].

When a diverging beam is incident on a bent crystal the path of any particle becomes a tangent to the bent crystallographic planes in some region in the interior of a crystal. Volume capture into the channelling mode is then possible for particles incident within the limits of the whole bending angle of the crystal. Volume capture of protons of 1 GeV energy within an angular range of several milliradians in a silicon crystal bent to $R = 46$ cm was observed experimentally at LINP in 1982 [19]. The relationships governing this effect in bent crystals have been investigated in detail at IHEP at the energy of 70 GeV [48]. It has been established that the probability w of volumn capture is directly proportional to the bending radius R (Fig. 10). A comparison with the results of Ref. [19] has led to the conclusion [48] that w varies with momentum as $p^{-3/2}$. A theoretical analysis of volume capture [35, 47, 49] carried out on the basis of transport equations or computer simulation (see also Section 2.6) has shown that the usual multiple scattering mechanism is sufficient to account for the experiments [19, 48]. Following Ref. [47], a simple analytic estimate of the probability w can be obtained and it explains the origin of the experimental dependence $w \propto R/p^{3/2}$.

The characteristic length L_D governs the probability w of a transition from the channelled fraction of a beam to the unchannelled one, $w \approx \delta z/L_D$, in a distance δz. It follows from the rule of reversibility that the probability of a reverse transition from an unchannelled fraction to a channelled one is the same quantity w. In a bent crystal an unchannelled particle rapidly loses its orientation relative to the bent channel. Misorientation by an angle of the order of the critical value θ_c occurs in a distance of the order $R\theta_c$. Therefore, the probability of a transition to

the channel during the whole interaction time is of the order of

$$w \approx \frac{R\theta_c}{L_D} \propto \frac{R}{p^{3/2}} . \quad (26)$$

This formula follows in fact from the principle of reversibility and is supported, to within a factor of ~ 2, by the experimental results [19, 48]. It should be pointed out that the reversibility rule, which provides good grounds for understanding the experiments, leaves no hope of the use of rechannelling for increasing the efficiency of a crystal. The diffusive nature of the scattering processes can only equalise the densities of states in a channel and outside it, so that the efficiency of volume capture cannot exceed the efficiency of end-face capture. The same conclusion can be drawn from expression (26). The intensity of a beam captured from the end face is $N_{ec} \approx \theta_c f_0$ (f_0 is the phase density or the 'brightness' of the incident beam). In the case of volume capture the quantity wf_0 has to be integrated over the whole range of capture angles Φ:

$$N_{bc} = \int \frac{R\theta_c}{L_D} f_0 \exp\left(-\frac{R\phi}{L_D}\right) d\phi = \theta_c f_0 \left[1 - \exp\left(-\frac{R\Phi}{L_D}\right)\right]. \quad (27)$$

The existence of the exponential factor is of fundamental importance and takes into account the dechannelling along the length of a crystal. Hence, it is clear that volume capture may compete with end-face capture only in the case of a wide beam and large bending radii $R\Phi \geqslant L_D$, but the former can never exceed the latter in brightness because of the onset of dynamic equilibrium (dechannelling and rechannelling balance out). In the case of narrow beams characterised by $R\Phi \ll L_D$ the ratio $N_{bc}/N_{ec} = R\Phi/L_D$ increases linearly with increase in the beam divergence, which is also self-evident.

2.5.1 Gradient mechanism of volume capture

The possibility of capture of above-barrier particles in the dechannelling mode, even in the absence of scattering, in a crystal with a variable bending radius was first considered in Ref. [50]. The equation of motion of a 100 GeV proton was solved numerically for a silicon crystal in which the curvature $1/R$ decreased abruptly to 0 at a depth of 10 or 20 μm ($\lambda \approx 30$ μm). It was concluded that volume capture is possible where the curvature of a crystal decreases abruptly.

The general case of the interaction of a charged beam with the potential of a crystal of variable curvature was considered in Ref. [51]. The existence of volume capture was predicted for the potential of planar channels with a continuously decreasing curvature in the beam direction. This is known as the 'gradient capture' and it is the reverse of the centrifugal dechannelling process (Section 2.2), just as the volume capture by scattering is the reverse of ordinary dechannelling (Section 2.3). In fact, the existence of two feed-in mechanisms, which are the reverse to the two well-known feed-out mechanisms, is a consequence of the general rule of reversibility of particle paths in a crystal. The following expression is derived in Ref. [51] for the gradient capture efficiency:

$$w_{gr} = \frac{R'\lambda}{2R}\left(1 - 2\frac{\langle x\rangle}{d_p}\right) , \quad (28)$$

where $R' = dR/dz$ is the gradient of the radius of curvature and $\langle x\rangle$ is the transverse coordinate (relative to the channel centre) averaged over a period. In the case of weakly bent crystals the quantity in the parentheses differs little from unity. In the harmonic approximation the expression (28) becomes

$$w_{gr} = \frac{R'\lambda}{2R}\left(1 - \frac{R_c}{R}\right) . \quad (29)$$

We can use the above expression to show [51] that the integral efficiency of particle capture from a beam with a wide angular distribution is equal to the efficiency of the end-face capture of the same beam, irrespective of the nature of the function $R(z)$. This conclusion is valid also in the general case of an arbitrary potential and this is a consequence of the Liouville theorem. In the absence of dissipation processes the phase density of the captured beam is identical with the phase density of the incident beam.

The first experimental evidence of the gradient effect in the volume capture of protons of 70 GeV energy was reported in Ref. [48] and the magnitude of the effect was approximately twice that predicted by expression (28). An increase in the momentum causes w_{gr} to increase as $\lambda \propto p^{1/2}$, whereas the quantity given by expression (26) falls as $1/p^{3/2}$. In other words, the influence of the centrifugal effects on the channelling increases and the influence of the scattering falls as p is increased. For this reason the ratio of the efficiencies of the two volume capture mechanisms changes in favour of the gradient mechanism at high energies.

2.6 Computer simulation of channelling

The channelling in bent crystals was simulated by A M Taratin et al. [52]. Their model is still based on the diffusion approximation. A particle makes a small step δz in accordance with Eqn (10). The average energy loss $\langle \delta E\rangle_s$ in close collisions with electrons is calculated for this step. The expression (20) relates $\langle \delta E\rangle_s$ to the mean-square angle of the scattering of a particle in these events. The scattering is simulated in accordance with the Gaussian distribution. Multiple scattering on nuclei is simulated similarly.

Although the diffusion approximation is in reasonable agreement with the experiments, computer simulation does not in principle need the approximations involving averaging or the assumption that the scattering is weak. The energy transferred in close collisions with electrons fluctuates strongly and may be sufficient to scatter a particle in one event through an angle comparable with θ_c. Close collisions not only influence the scattering processes but also determine the spectra of the particle energy losses dE/dz. These spectra have interesting features in the case of aligned crystals (see, for example, Ref. [53]): the average value and the scatter of the losses dE/z experienced by channelled particles are considerably less than the corresponding values for misoriented crystals. This feature is used widely in experiments to select the channelled particles in accordance with dE/z in solid-state detectors built into a crystal; it has been used recently to align the H8 beam channel at CERN [25] in order to ensure the minimum divergence of $\sim \pm 3$ μrad of a beam on a crystal. The sensitivity of the method is ~ 1 μrad, which is considerably better than any of the standard techniques. Finally, fluctuations of the energy losses may be important in

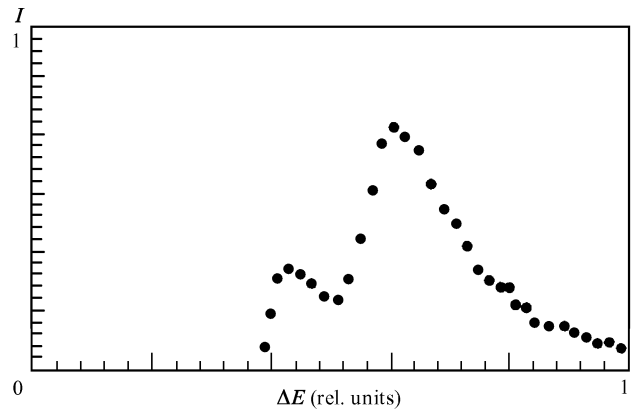

Figure 11. Spectrum of the energy losses experienced by protons in an oriented crystal, obtained by CATCH simulation under the experi-mental conditions of Ref. [56].

the dynamics of particles in an accelerator (in the task of particle *extraction* by a crystal) since the stability of particle motion in a ring is very sensitive to the losses. An example of a program which satisfies these conditions is CATCH [54] in which an account is taken of the probability of the scattering by electrons with a large energy transfer T in one event. The scattering is simulated in accordance with the distribution function

$$\frac{\mathrm{d}^2N}{\mathrm{d}z\,\mathrm{d}T} = \frac{2\pi N_\mathrm{A} r_\mathrm{e}^2 m_\mathrm{e} c^2 Z_i^2 Z \rho}{A\beta^2 T^2} \frac{n_\mathrm{e}(x)}{n_\mathrm{am}} \,. \tag{30}$$

Fig. 11 shows an example of the $\mathrm{d}E/z$ spectrum simulated by the CATCH program for the experimental conditions given in Ref. [56]. Such splitting of the spectrum into the 'channelled' (with anomalously low values of $\mathrm{d}E/\mathrm{d}z$) and 'unchannelled' (high values of $\mathrm{d}E/\mathrm{d}z$) fractions has been used in the experiments [14] to separate the channelled particles from the background. Simulation [57] of this experiment repeats exactly this procedure. Protons are selected on the basis of low losses ΔE in the straight front part of a crystal and their angular distribution behind the crystal is fitted to an exponential function. The results obtained for L_D are plotted in Fig. 6. The simulation results agree with the measurements to within $\approx 10\%$; moreover, the dependence on the temperature of a crystal is reproduced correctly. This experiment has been simulated earlier [58], but without selection on the basis of $\mathrm{d}E/\mathrm{d}z$.

Simulation of the volume capture process can be illustrated by considering Ref. [39]. Volume capture of 70 GeV protons and their subsequent dechannelling in bent (110) and (111) silicon crystals was observed experimentally. In the interior of a crystal, corresponding to exit angles of 6–18 mrad, the dechannelling was exponential in the experiments and in the simulation. The following lengths L_D were obtained:

$$L_{\mathrm{D,exp}}^{(110)} = 37 \pm 5\,\mathrm{mm}\,, \quad L_{\mathrm{D,exp}}^{(111)} = 52 \pm 2\,\mathrm{mm}\,,$$

$$L_{\mathrm{D,sim}}^{(110)} = 39 \pm 3\,\mathrm{mm}\,, \quad L_{\mathrm{D,sim}}^{(111)} = 40 \pm 4\,\mathrm{mm}\,.$$

It is also interesting to compare the probabilities of volume capture by 'stable states' which decay exponentially. Table 1 lists the probabilities found experimentally, by simulation, and on the basis of the $w \approx R\theta_\mathrm{c}/L_\mathrm{D}$ model. The beam deflection efficiency has been investigated by simulation and experiment [59]. A beam of 450 GeV/c protons was deflected in an Si(110) crystal by angles from 3 to 8.5 mrad. The low beam divergence, $\sigma \approx 15$ μrad, was the reason for the high efficiencies listed in Table 2. Simulation of the extraction of a proton beam from an accelerator will be discussed in Section 5.

Table 1. Probability (%) of bulk capture into 'stable states' deduced from experimental results [48], from computer simulation [39], and from a model [47].

Crystal	Mode[47]	Simulation[39]	Experiment[48]
111	0.13	0.17 ± 0.02	0.23
110	0.18	0.23 ± 0.02	–

Table 2. Efficiency of deflection of 450 GeV/c protons by an Si(110) crystal found experimentally and by simulation (all results taken from Ref. [59]). The upper row of values applies to the whole beam and the lower row applies to the particles incident within the angular interval $\pm\theta_\mathrm{c}$. Only the statistical errors are shown.

		Deflection by angle/mrad		
		3.0	5.7	8.5
Efficiency (%)	Experiment	20.2 ± 2	10 ± 1	7.7 ± 0.3
	Simulation (σ=15 μrad)	20.9 ± 0.8	15.2 ± 0.5	8.8 ± 0.5
Efficiency (%) in interval $\pm\theta_\mathrm{c}$	Experiment	54 ± 2	33 ± 5	16 ± 3
	Simulation	56 ± 4	39 ± 2	26 ± 2
$\pm\theta_\mathrm{c}$	Simulation	56 ± 4	39 ± 2	26 ± 2

3. Deflection and focusing of beams by crystals

The following questions must be answered before attempting practical use of single crystals in accelerators. What is the maximum intensity of a beam and what are the angles by which a beam can be deflected in a crystal? What are the margins of the mechanical and radiation strengths which are required? Does the crystal unbend as a function of temperature and radiation? What should be the length of a perfect crystal? How does the quality of crystal bending and of its surface treatment affect the characteristics of the deflected beams?...

Much work has been done at IHEP with the aim of answering these questions. In the course of this work tens if not hundreds of crystals have been bent and tested in beams.

3.1 Requirements imposed on the quality of single-crystal slabs and bending devices

Effective bending of high-energy particle beams requires a high quality of the orientation and treatment of the faces of single-crystal slabs. In the reported experiments on 70 GeV proton beams a crystal with a length of about 100 mm and ≈ 1 mm thick should have an effectively deflecting layer which is close in dimensions to the total cross section of the crystal. This can be achieved if the orientations of the slabs are accurate to within $\sim 1'$ and if the side faces are parallel

and plane to within 10 μm over the whole length of the crystal. The depth of the crystal layer disturbed by polishing the side faces should be of the same order of magnitude. In principle, these requirements can be satisfied by the use of existing technologies.

In the planned use of crystals in teraelectron-volt accelerators, especially in the case of a beam extraction from super-conducting colliders, the requirements in respect of the quality of orientation and surface treatments are even more stringent. For example, the impact parameter of a beam incident on a crystal used to extract the beam from the LHC collider must be a fraction of a micron [77], which requires new techniques for the monitoring and treatment of crystal surfaces. When the energy of the deflected particles increases to the teraelectron-volt range, the requirements in respect of the quality of single-crystal slabs also become more stringent. The mosaic regions on crystals should not be larger than ~ 1 μrad and this value is governed by the critical channelling angle.

According to the familiar empirical rule a silicon slab of thickness H can be bent elastically to form a cylinder of radius R if $R > 1000H$. However, efficient bending of beams requires that the bending radius should have the optimal value R_{opt} which in the case of large bending angles is equal to several critical radii R_c [40]: $R_{\text{opt}} \sim (3-5)R_c$. In the case of silicon we have $R_c/\text{m} = 0.0018E/\text{GeV}$. Therefore this mechanical strength criterion limits the thickness of the slabs used: $H/\text{mm} \leqslant 0.007E/\text{GeV}$. For example, if the energy of the particles being deflected is $E = 70$ GeV, the optimal deflection is produced by a slab which is $H \leqslant 0.5$ mm thick. However, for teraelectron-volt accelerators currently under construction the slab thickness may be just tens of millimetres, which is as a rule much greater than the characteristic dimensions of a beam.

Bending a crystal to form a given surface is in general a difficult task. Bent crystals have been used in the past for the focusing of x-rays and gamma rays in crystalline diffraction devices employed in nuclear spectroscopy. Two general approaches have been used to deal with this problem [81]: (1) bending by cylindrical mirrors; (2) the method of moments.

Elastic bending of a single-crystal slab is considered in Ref. [82] for two ideal cases: the method of moments and cylindrical mirrors. This is done on the basis of the theory of elasticity of anisotropic bodies. It is shown that a slab is bent not only in the longitudinal direction, but experiences torsion in a transverse direction, so that it assumes the shape of a saddle or of a barrel, or (as a special case) a cylindrical shape. This depends on the actual anisotropy of a crystal. Additional moments may be induced by a real crystal holder so that the bending may be more complex and this is particularly true at the slab edges.

The specific nature of the requirements which bent crystals must satisfy in order to be useful in the deflection of beams of high-energy particles, which distinguish this case from the use of such crystals in the focusing of gamma rays, are related to the different directions of the particle paths: gamma rays enter the slabs normally to the large faces and charged particles move along cut slabs. Therefore, the requirements in respect of the constancy of the bending radius along the longitudinal coordinate are as a rule not very stringent (it is sufficient to ensure that the error does not exceed $\Delta R/R \sim 1\%$). However, there are specific requirements that have to be satisfied at the edges of the bent slabs. It is necessary to maintain the total bending angle Θ within the angular acceptance of the existing magnet-optical particle transportation channels to which beams have to be deflected. Usually, the limits are $\Delta\Theta = 0.1$ mrad. This precision may be monitored by reflecting a laser beam from a crystal moving linearly on a micrometer stage.

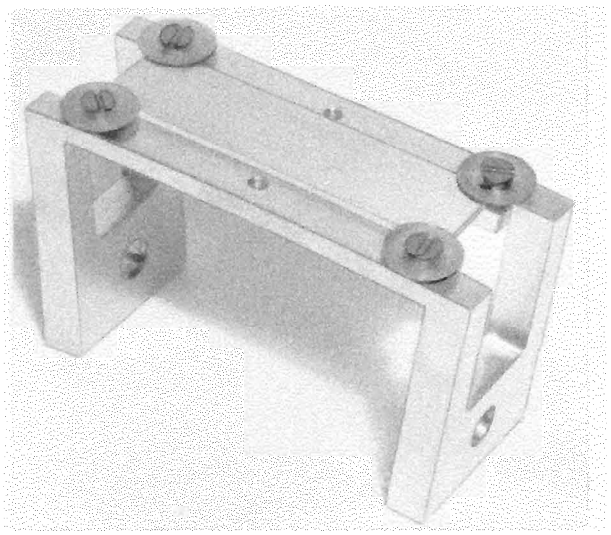

Figure 12. Device for bending and clamping a crystal.

Experiments show that a major problem is the avoidance of bending nonuniformity along a transverse coordinate. In undemanding cases, when crystals are used to split an extracted beam, it is sufficient to ensure that the error does not exceed $\Delta\Theta_\perp \approx 0.1$ mrad, which is usually considerably less than the divergence of the incident beam ($\sim$1 mrad). In the case of beam extraction from large accelerator colliders or in the study of the efficiency of particle capture into the channelling mode such an error is unacceptable and it is governed by the critical channelling angle. In this case the edges of a crystal should be left flat. Alternatively, the quality of bending can be checked by laser interferometry and the surfaces of the bending mirrors may be corrected.

These or other methods for the bending of a crystal are used in experiments on the deflection of high-energy particle beams. Fig. 12 shows a widely used bending device [18]: it is based on a metal mirror and it is known in the literature as the 'bridge' (see, for example, Ref. [90]). The central part of the bridge is free of matter in order to minimise the particle losses. The crystal is clamped to the bent metal surface by elastic discs which act as sprung supports that relieve the mechanical stresses generated as a result of the interaction of a high-intensity beam with a crystal.

3.1.1 Requirements which have to be satisfied by goniometric devices

The minimal angular displacement step, comparable with the critical channelling angle ($\sim$25 μrad at 70 GeV) is required in the alignment of crystals. This can be achieved with the aid of a familiar compact structure which includes a lever set in motion by a micrometer screw attached to the axle of a step motor. Depending on the size of the lever and the micrometer screw gauge, such structures can ensure that the angular displacement step is 8–30 μrad.

A similar structure with an angular step of 4 μrad has been used at CERN [29, 30]. Specialists are of the opinion that it should be possible to reduce this step to less than 1 μrad, which will be necessary in the teraelectron-volt energy range.

3.2 Investigations of main potential applications of crystals in beam handling

3.2.1 Observations of beam deflection in crystals made of different materials

Expression (22) for the dechannelling length leads to the following dependence on the properties of a crystal: $L_D \propto a_{TF} d$, which in the case of isomorphous crystals leads to $L_D \propto Z^{-1/3}$ (slow fall on increase in Z). However, since the critical bending radius obeys $R_c \propto Z^{-1}$ (which is a quantity reciprocal to the critical field), the 'strength' of a deflector $\Theta_D \propto L_D/R_c \propto Z^{2/3}$ increases strongly with increase in Z. Moreover, the critical capture (channelling) angle $\theta_c \propto \sqrt{U_c} \propto Z^{1/3}$ also increases. Therefore, in principle, heavy-atom materials are preferable for beam bending.

Experience shows however that at high energies the main factor governing the use of crystals is still the quality of the crystal structure. In this respect silicon is the best material. The high quality of this material is supported by the measured dechannelling lengths (Section 1) and by some of the experimental results on the deflection of beams in long crystals.

For example, tests have been recently carried out on a (110) silicon crystal, 150 mm long, bent to an angle of 20 mrad. The fraction of the particles deflected by this crystal agrees with calculations confirming its high quality.

In these tests a comparison has been made of the deflecting properties of long (up to 100 mm) silicon crystals obtained from different sources. It has been found that the results are reproducible to within 5% from crystal to crystal and this value is equal to the measurement error.

Even silicon slabs produced on a large scale, cut from a large-diameter ingot for the fabrication of microcircuits, have good bending properties. In one of the experiments a slab 100 mm in diameter had the (111) orientation, n-type conduction, and a dislocation density not exceeding 100 cm^{-2}. Made into a deflector 30 mm long, this crystal deflected 90% ± 5% of the particles that were deflected by a dislocation-free 'standard'.

As pointed out above, dislocations are the greatest hazard at high energies because the dechannelling cross section of defects of the other types either falls or remains constant when the particle energy is increased [7]. Fig. 13 gives the theoretical curves showing the reduction in the dechannelling length of 70 GeV particles on increase in the dislocation density in a crystal. The upper curve is the approximation based on single scattering [61] and the lower curve is based on the transport approach [83]. There is also an experimental point in this figure, which represents a reduction in the dechannelling length in an imperfect silicon crystal on the assumption that the number of defects in this crystal agrees with the value given by the supplier.

Other materials are much inferior to silicon. Several germanium crystals up to 45 mm long have been tested. The nominal dislocation density in the best samples has been below 1000 cm^{-2}. The fraction of deflected particles and a comparison with silicon crystals under identical conditions have yielded estimates of $L_D \sim 5$ mm (this point is plotted in Fig. 13).

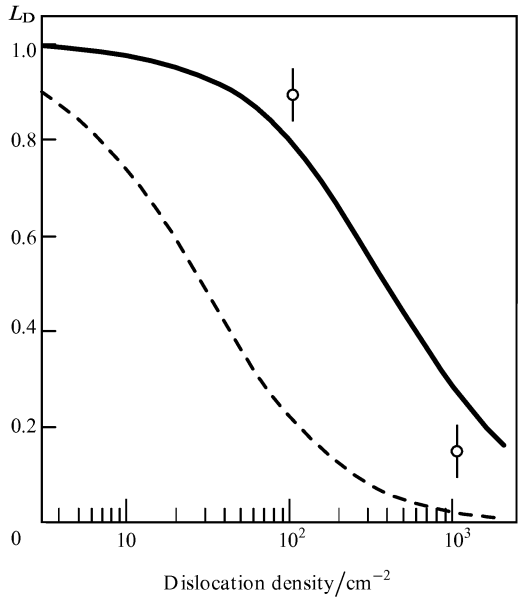

Figure 13. Dependence of the dechannelling length L_D at 70 GeV on the dislocation density in a crystal. The curves represent theoretical models and the points are experimental values.

It is obvious that in the search for new materials suitable for the channelling of high-energy particles it is necessary to determine the crystal quality by nonchannelling methods before experiments are started with a beam. It is probably preferable to synthesise new crystals with a 'perfect' structure rather than search among the existing materials.

3.2.2 Formation of a high-intensity beam

In the first (1979) experimental tests of the idea of particle deflection by a bent single crystal [16], the deflected beam intensity was barely several particles per second. The low efficiency of particle deflection by crystals (mainly because the beam emittance did not match the crystal acceptance) and radiation damage to semiconductor crystals have led to the opinion that this beam handling method is of limited use.

Special experiments have therefore been carried out to test the feasibility of formation, by a single crystal, of an intense proton beam sufficient in principle for the generation of secondary-particle beams [84].

In these experiments a silicon crystal bent by 13 mrad was placed in a 70 GeV proton beam extracted from an accelerator. Part of the beam was captured into the channelling mode and deflected to a magnet-optical channel where detectors were located. The silicon crystal had the (111) orientation and its dimensions HVL (horizontal width, vertical height, and length along the beam) were 0.5 mm, 40 mm, and 30 mm, respectively. The length of the bent part was 20 mm and the average bending radius was 1.5 m. The beam aimed at the crystal had the intensity 1.3×10^{13} per cycle; it was rapidly extracted (in 5 μs) and the cycle repetition period was 9 s. The beam dimensions were $\sigma_x = \sigma_y = 1.4$ mm and the angular divergence in the x plane (beam bending plane) was $\sigma_\theta = 0.8$ mrad. In one cycle about 1.8×10^{12} particles

directly reached the end face of a crystal and the time-average value of the released power was ~ 1 W. The crystal was heated by the beam to ~ 150 °C. Moreover, it was subject to a dynamic mechanical stress at the moment of passage of the beam. The first attempts to deflect a rapidly extracted intense beam in this single crystal were unsuccessful. The crystal bent by bonding to a metal cylinder over the whole of its surface fractured under dynamic stresses. However, success was achieved when the crystal was pressed against a metal base by sprung supports (Fig. 12).

The crystal bent a maximum of 9.5×10^9 particles per cycle. The particle losses from the main beam were of the order of 1%, which was approximately 10 times the intensity of the deflected beam, i.e. the efficiency of beam splitting by the crystal was $\sim 10\%$. For the parameters of the incident beam given above, when the angular divergence was ~ 40 times greater than the critical channelling angle, this efficiency was in agreement with the calculations.

Fig. 14 gives the time dependence of the intensity of the deflected beam from the beginning of the operation of the crystal (at its optimal position). The intensity fluctuations from one cycle to the next were within the acceptable limit of 12%. At this fluctuation level no changes were found in the average intensity, confirming the optimistic theoretical predictions [40, 58] of a weak temperature dependence of the deflecting properties in the case of planar channelling.

The spatial stability of the deflected beam was monitored by a remote ionisation chamber. The change in the bending angle of the crystal was $\Delta\Theta/\Theta < 10^{-2}$.

The irradiation of the crystal by the rapidly extracted intense beam was continued during one run of the accelerator. The crystal not only withstood a flux of $\sim 10^{19}$ cm^{-2} particles under thermal and mechanical stresses (it did not fracture), but it also retained the channelling properties without any significant deterioration.

These results were unexpectedly very promising. They demonstrated that crystals may be used for years in the usual magnet-optical channels.

3.2.3 Beam deflection by large angles

It should be pointed out that bent single crystals are also suitable for the experimental work on teraelectron-volt accelerators, because they can deflect beams through much larger angles than conventional electromagnets. As pointed out in the preceding sections, the 'strength' of a crystal deflector is $\Theta_D = L_D/R_c$. Since both L_D and R_c increase almost identically (linearly) when E is increased, the maximum possible angle of deflection of a beam by a crystal is independent of the particle energy. This is an important advance of crystal optics. The results of measurements of L_D, given in Section 2, indicate that in the case of Si(111) and Si(110) the values of the deflector 'strength' are $\Theta_D = 0.47$ and 0.34 rad, respectively.

The ability to deflect a beam through a large angle has also been confirmed on an extracted beam of 70 GeV protons. This experiment had been carried out analogously to that described above, but the silicon crystal was bent by $\Theta = 130$ mrad (a record value so far). Its width, height, and length along the beam were 0.5 mm, 15 mm, and 100 mm, respectively. In the optimal orientation the crystal deflected $\sim 10^8$ protons per cycle.

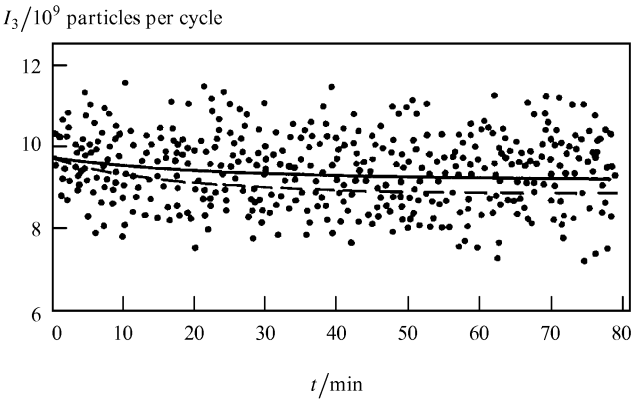

Figure 14. Time dependence of the intensity of a beam deflected by a crystal which is at the optimal position. The continuous curve fits the experimental points and each of these points represents one acceleration cycle. The dashed curve is calculated taking into account the temperature dependence of the channelling properties.

In the deflection of particles of teraelectron-volt energies through such angles it is necessary to have perfect crystals several tens of centimetres long. There are also grounds for optimism in respect of the solution of this problem: crystals 15 cm long have already been tested in a beam (see Section 3.2.1).

3.3 Beam focusing by a crystal

3.3.1. Focusing method

Bent crystals not only can deflect a beam, but also focus it. In principle, there are several ways of doing this. One of them is the focusing of a beam by a thin bent crystal oriented normally to the crystallographic planes [85].

Another possible approach is based on the deformation of planes in a thick crystal when it is compressed. A shortcoming of these two methods is the presence of a background of the unchannelled fraction of the beam.

In the middle eighties A I Smirnov (LINP) put forward a promising method for focusing a parallel beam into a line and simultaneously deflecting the beam through a considerable angle, so as to form 'clean' focused beams.

In this method the surface of the exit face of a bent crystal is shaped so that the tangents to the crystallographic planes on this surface pass through the same line and, consequently, the particles in the deflection plane are collected in a line focus because of the difference between the deflection angles [86]. When the crystallographic planes are bent to form a cylinder of radius R (Fig. 15), it is essential to ensure that the line formed by the centres of curvature OO′ is located on the surface of a cylinder of radius r representing the shape of the exit face of the crystal. The focal length f is then $f = (4r^2 - R^2)^{1/2}$.

In the case of ideal bending and shaping of a crystal the size of the beam Δx at the focal point is $\Delta x = 2f\theta_c$ and it is governed by its angular divergence within the limits of the critical channelling angle θ_c.

Since this critical angle is quite small ($\theta_c = 0.02$–0.002 mrad for particles of energies from 100 GeV to 10 TeV in the case of planar channelling in silicon) and the technology used to bend and shape a crystal makes it possible to achieve a focal length of the order of several centimetres, the attainable dimensions of the beam are ~ 10

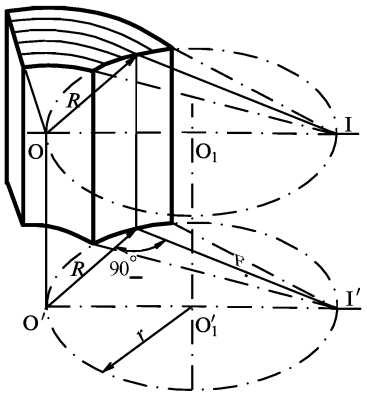

Figure 15. Principle of focusing of a beam by a crystal. OO′ is a line of centres of curvature of the crystallographic planes; O_1O_1' is the axis of a cylinder of radius r representing the shape which is imposed on the face of a crystal; I and I′ are the focal lines where tangents to the bent planes converge, deduced on the basis of the well-known geometry theorem.

μm for the gigaelectron-volt energies and ∼1 μm for the teraelectron-volt range. The linear magnification in the course of focusing is $q = 2f\theta_c/H$, where H is the characteristic thickness of a crystal (∼1 mm), and it can reach a fraction amounting to, respectively, hundredths and thousandths in the two energy ranges.

3.3.2 Focusing of a parallel beam to form a point in the particle deflection plane

The focusing method described above was implemented in a collaboration experiment involving IHEP and LINP: it was carried out on a 70 GeV proton beam [86, 87].

The specialists at the LINP developed a technology for bending a focusing crystal and made several focusing devices. Three silicon crystals were used: their width, height, and length along the beam were 2 mm, 15 mm, and 70 mm, respectively; the orientation was (111). The crystals were bent to form a cylinder of radius $R = 2.7$ m over a length of ∼65 mm. Different focal lengths were obtained by shaping the exit ends of the crystals to form cylinders with radii listed in Table 3 and the angles of cut of the focusing edge were varied in accordance with $\alpha = \arccos(R/2r)$ in the geometry of Fig. 15.

A proton beam of $\sigma_x = 2$ mm size with a small angular divergence $\sigma_{x'} = 0.1$ mrad was incident on a crystal placed on a goniometer stage. The orientational dependence of the signal produced by remote detectors was used to set the crystal in the channelling mode. The intensities of the incident and deflected (by an angle ∼24 mrad) beams were measured with scintillation counters. In the optimal orientation the crystal deflected 3% of the particles in the incident beam (which agreed with the calculations in which the beam and crystal parameters were taken into account).

The focusing effect was detected by nuclear photographic emulsions. Several emulsion layers were placed at different dis-tances from the exit face of a crystal. The exposed emulsions obtained for crystal No. 1 were analysed with a microphotometer and in the case of crystals Nos 2 and 3 a direct count was made of the distribution density of tracks over the cross section of the beam under a microscope. The size of the developed grains in a track ('track width') was about 1 μm.

Fig. 16 illustrates the focusing effect produced when the beam was bent in crystal No. 1. Fig. 17 shows the image of a beam focused by crystal No. 3 at a distance of 0.5 m (strongest focusing). Images of the beams focused in crystals Nos 2 and 3, magnified under a microscope, are

Table 3. Characteristics of focusing crystals and beam dimensions at the focus.

Crystal No.	R/m	r/m	α/deg	f/m	Focus size $2\sigma_x$/μm	
					calc.	meas.
1	2.7	2.21	58.2	3.5	175	200
2	2.7	1.52	30.4	1.4	70	80
3	2.7	1.374	11.9	0.5	25	43

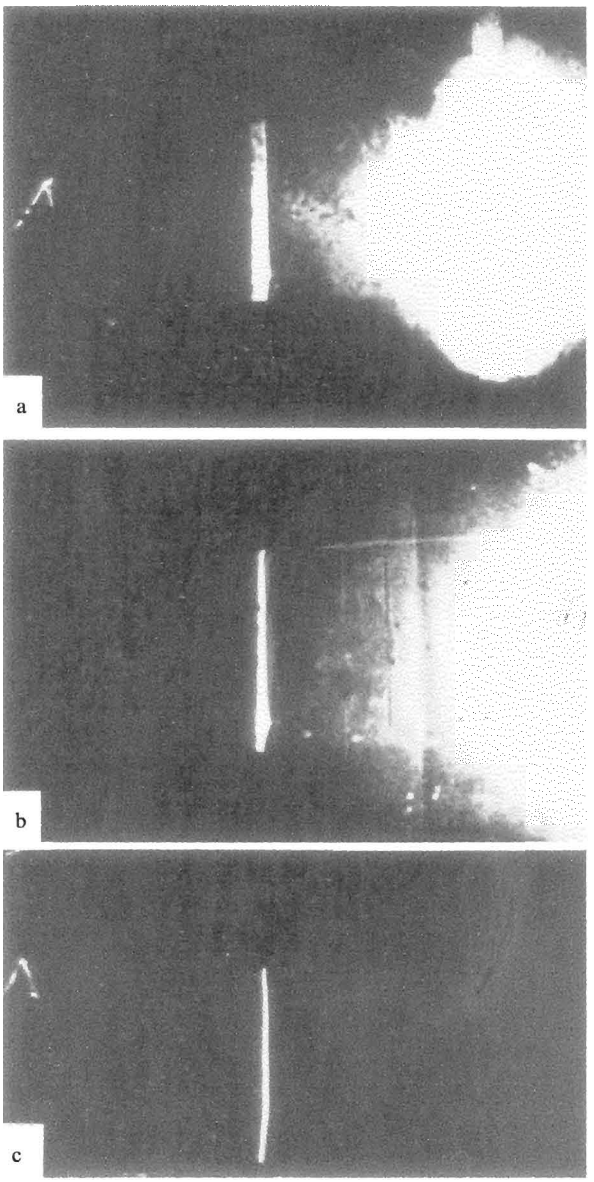

Figure 16. Image of the beam deflected by crystal No. 1, recorded in three emulsions at distances of (a) 0.7 m , (b) 2 m , and (c) 3.5 m from the crystal. The undeflected beam with a halo of secondary particles and a tail of particles dechannelled in the bent part of the crystal are shown on the right.

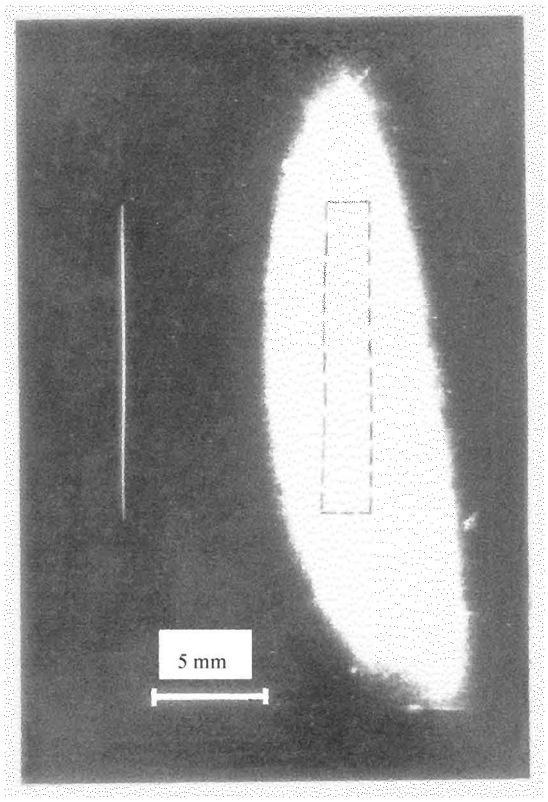

Figure 17. Image of the beam focused by crystal No. 3. The profile of the deflected and focused beam can be seen on the left. The dashed rectangle on the right is the cross section of the crystal.

given in Fig. 18. The beam dimensions $2\sigma_x$ at the crossover (calculated and measured) are listed in Table 3. It is evident from this table that for crystals Nos 1 and 2 the dimensions agreed to within 15%. In the case of crystal No. 3 the beam size at the crossover was considerably greater than the calculated value, which was due to an increase in the contribution of aberrations when the focal length was reduced.

This focusing method can be used to form particle beams of micron dimensions in the teraelectron-volt range when a new generation of accelerators is used. In this method the image of a beam deflected by a crystal can be simply transferred to an experimental setup by optics with the magnification of unity.

Another important application of crystal focusing devices involves the reverse direction of motion of particles (focusing from a point into a parallel line). An internal target in an accelerator, in the form of a filament located at the focus of a crystal, can in principle be used to collect and extract from a vacuum chamber a major part (~50%) of the secondary particles generated by this target. Estimates indicate that this method can be used to form beams of particles of $\sim 10^8$ s^{-1} intensity in large collider accelerators.

4. Applications of crystals to beams extracted from large accelerators

4.1 Beam attenuator

One of the first applications of crystals in accelerators has been their use as the deflecting components in magnet-optical beam lines. For example, the work done at the

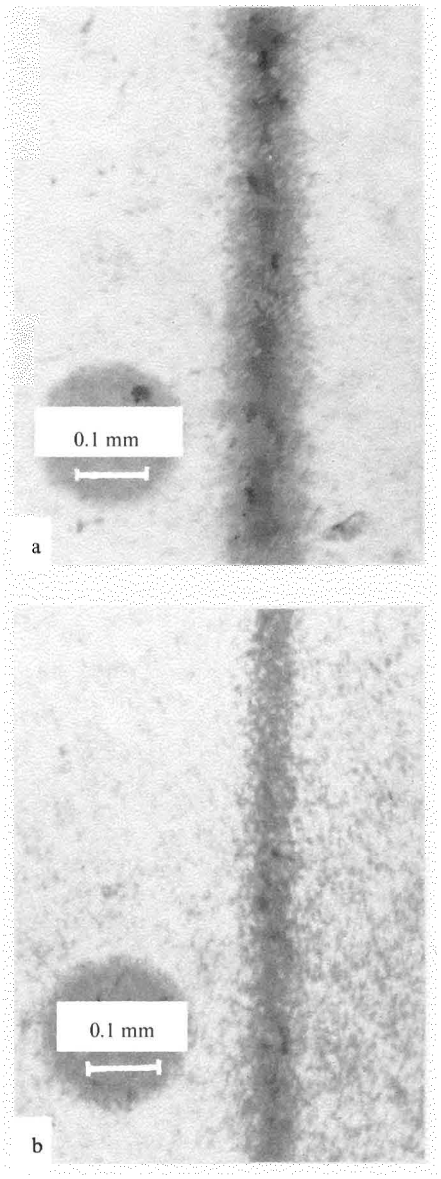

Figure 18. Images, magnified by a microscope, of a focused beam formed by: (a) crystal No. 2 (focusing at 1.4 m); (b) crystal No. 3 (focusing at 0.5 m).

FNAL reported in 1986 [21] involved the use of a crystal to form a low-intensity proton beam which reached an emulsion spectrometer. These experiments demonstrated for the first time that 800 GeV beams can be deflected.

A silicon crystal 26 mm long, placed in a beam line, replaced a pair of dipoles with an angle of rotation $\Theta = 3.7$ mrad and deflected part of the incident beam with $10^8 - 10^9$ cycle^{-1} in the direction of an emulsion spectrometer: the intensity of the deflected beam was $10^4 - 10^5$ cycle^{-1}. The undeflected beam was quenched in an absorber.

The reports of this experiment stressed several positive features of the use of crystals as beam attenuators, compared with collimators. The conventional collimators can reduce the intensity by a factor of 10–100. Such collimators are heavy and therefore difficult to control. Moreover, they become sources of secondary particles and create a halo.

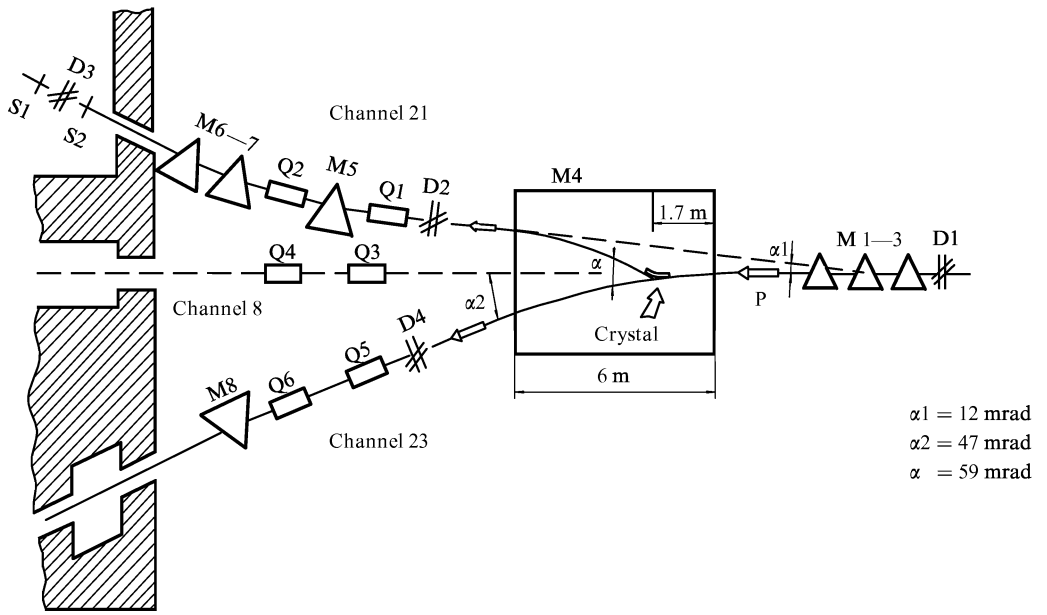

Figure 19. Layout of the station for splitting an extracted proton beam in the beam lines of the accelerator at the Institute of High-Energy Physics. Here, M1–M9 are bending electromagnets; Q1–Q6 are quadrupolelenses; D1–D4 are multichannel beam profilometers; S1–S2 are scintillation counters.

The real efficiency of the deflection of a beam by a crystal was found to be $\eta = 0.54 \times 10^{-3}$. A theoretical estimate, which took into account the dechannelling factors (≈ 0.27) and the ratio of the crystal acceptance to the beam emittance ($\approx 1.2 \times 10^{-2}$), was $\eta_m = 3.2 \times 10^{-3}$.

The authors attributed the lower efficiency to the non-optimal position of the crystal along a coordinate, a possible underestimate of the dechannelling effects, and a possible loss of particles through side faces (because of inaccurate cutting of a slab). In spite of this, the experiments showed that bent crystals in accelerators are not exotic devices, but an important tool in high-energy physics.

Bent single crystals of similar quality have been used later in the U-70 accelerator at IHEP [18] and in the Super Proton Synchrotron (SPS) at CERN [88].

4.2 Beam splitting

The improvements in the technology of bending of crystals have subsequently made it possible to split an extracted proton beam, so that several physical experiments could be carried out simultaneously.

Usually a beam is split by an electrostatic or a magnetic splitter [89]. This is a technically fairly complex approach requiring considerable space, since the angles of deflection of a beam by a conventional splitter are very limited. The use of crystals provides a simple means for beam splitting, which is unattainable by conventional techniques.

The task of beam splitting has become particularly topical in the case of the 70 GeV accelerator at IHEP, where several magnet-optical particle channels were constructed in the eighties. This followed the commissioning of an accelerator booster and an increase in the accelerated beam intensity to more than 10^{13} protons per cycle.

The first crystal beam-splitting station [18] began to operate at the end of 1988; it is shown schematically in Fig. 19. In the first tests a proton beam of 5×10^{11} cycle^{-1} intensity, extracted slowly from the accelerator, was transported to a target in a setup intended for the study of processes in a tagged-neutrino beam. A silicon single crystal bent to an angle of 60 mrad deflected part of a moderate-intensity beam to a magnet-optical channel aimed at a target in a setup designed for hadron studies. The path of the channelled beam was aligned along the axis of the existing magnet-optical channel by placing the crystal deflector inside a 6 m bender magnet M4.

The process of aiming the beam on the crystal was aided by secondary-particle monitors and a television observation system. The primary proton beam was monitored by multichannel secondary-emission profilometers D1 and D4. The parameters of the deflected beam were measured with proportional chambers D_2 and D_3, operating in the charge integration mode, and by scintillation counters S1 and S2 connected in coincidence. This combination of analogue and counting methods for the detection of particles made it possible to determine the beam intensity over a wide dynamic range of $1-10^8$ particles per cycle.

Several different crystals were used as the deflectors: they included two silicon crystals, cut along the (111) crystallographic plane, and one germanium crystal cut along the (110) plane. The dimensions of the crystals were as follows: 0.5 mm, 15 mm, 60 mm for Si-1; 0.55 mm, 15 mm, 60 mm for Si-2; 0.6 mm, 15 mm, 45 mm for Ge. The considerable length of the crystals was due to the requirement of a fairly large bending angle (as pointed out in Section 2.5.1, for each bending angle there was an optimal bending radius and length: if the crystal were too short, the particles would become dechannelled because of the centrifugal effect, but if it were too long, a strong scattering would occur on electrons and nuclei, i.e. the conventional dechannelling would prevail).

Crystals were bent in the device shown in Fig. 12. The first tests established that a crystal could be used to split a beam of protons under working conditions in the magnet-optical channels $I_{23} = 10^{13}$ cycle^{-1}, $I_{21} = 10^7$ cycle^{-1}; this was achieved when a crystal was placed in the halo region of

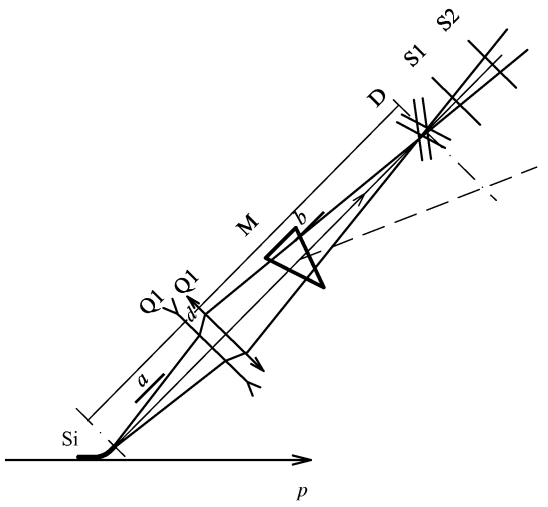

Figure 20. System for measuring the beam characteristics. Here, Si is a bent single crystal, D is an analogue ionisation chamber; S1 and S2 are scintillation counters; Q1 and Q2 are quadrupole lens doublets; M is a bender magnet. The continuous lines are the paths of the rays in the horizontal plane and the dashed line is the dispersion.

the beam so that the particle losses did not exceed a permissible limit of $\sim 10^{10}$ cycle^{-1} ($0.1\% I_{23}$).

Subsequent experience demonstrated a high reliability of the crystal beam-splitting station. The Si-1 silicon crystal worked without replacement for five years: it withstood a particle flux in excess of 10^{18} cm^{-2} and retained its deflecting properties without significant deterioration.

Several additional crystals were placed subsequently in the channels and these made it possible to operate simultaneously several experimental setups.

4.3 Beam diagnostics

The early work had already revealed that the ability of a bent crystal to modify a beam within a small phase volume $\varepsilon = 2\theta_c H$ (θ_c is the critical channelling angle and H is the thickness of a crystal) can be used for particle beam diagnostics. For example, it is reported in Ref. [21] that it is possible to measure the beam emittance by recording the particles deflected by a crystal when this crystal is rotated and displaced transversely relative to the beam.

It is demonstrated in Ref. [91] that a bent single crystal can provide full information on the beam characteristics (emittance, profiles, halo, momentum spread).

4.3.1 Measurement method

The setup used in measurements is shown in Fig. 20. A bent silicon single crystal is introduced into a high-intensity beam of high-energy particles: the coordinate of this crystal is x and its orientation is x'. The part of the beam deflected by the crystal is directed along the axis of a long magnet-optical system (lenses Q1 and Q2; magnet M) and it is recorded at the end of this system by an analogue ionisation chamber D and scintillation counters S1 and S2, used in coincidence. The acceptance of the magnet-optical system makes it possible to record all the deflected and channelled particles and to remove completely the background of secondary particles formed on interaction of the unchannelled fraction of the primary beam with the crystal matrix.

Under these conditions the number of particles recorded by the counters is

$$I(x,x') = \left[\int_{-H/2}^{H/2}\int_{-\theta_c}^{\theta_c} \rho(x,x')\,\mathrm{d}x\,\mathrm{d}x'\right]\eta_D(L,R,p)\ ,$$

where $\rho(x,x')$ is the phase density of the beam in coordinate–angle space and $\eta_D(L,R,p)$ is the dechannelling factor which depends on the length of the crystal, on the bending radius, and on the momentum of the deflected particles. In view of the smallness of the crystal acceptance, we can write down

$$I(x,x') = \rho(x,x') \times 2\theta_c H \eta_D\ ,$$

which leads to

$$\rho(x,x') = \frac{1}{2\theta_c H \eta_D} I(x,x')\ ,$$

i.e. the phase density of the beam at the point (x,x') is proportional to the number of particles deflected by the crystal provided only the increase in the temperature of the crystal caused by the beam heating does not significantly alter the channelling properties.

4.3.2 Determination of the spatial–angular characteristics of a beam

The method for measuring the beam characteristics described above was applied to one of the beam lines of the accelerator at IHEP. Part of a 70 GeV proton beam, trapped into the channelling mode, was bent by an angle of 13 mrad and directed into a beam line where the front optics is provided by the system shown in Fig. 20.

The phase density $\rho(x,x')$ was measured for an extracted beam of 3×10^{12} cycle^{-1} intensity. In Fig. 21a the results of measurements of $\rho(x,x')$ are plotted in the form of equi-potential lines in the (x,x') plane and these lines link the experimental points. These points are the results of angular scanning with the beam at each step of the displacement of the crystal along the horizontal. Five closed lines in this figure, counted beginning from the centre, enclose the beam volume at the levels of 0.75, 0.5, 0.25, 0.1, and 0.01 of the maximum density. The values of the beam emittance corresponding to these levels are (π mm mrad): 0.26, 0.68, 1.2, 1.6, 4.2, respectively.

Displacement of a crystal oriented optimally in respect of the angle made it possible to measure the value of $\rho(x,0)$, i.e. to determine the beam profile $N(x)$ in a wide dynamic range. The results of determination of the profile $N(x)$ extending down to 10^{-7} of the maximum are presented in Fig. 21b. It was possible to measure the halo of the high-intensity beam to such a very low level (10^{-7}) because of a clear orientational dependence of the useful signal generated by the detectors. When the crystal was misoriented by an angle exceeding the acceptance of the magnet-optical system, the channelled beam disappeared and it was therefore easy to distinguish this beam from the background signal.

4.3.3 Determination of the distribution of the particle momentum

The ability of a crystal to form a small-emittance beam in combination with spectrometric capabilities of the magnet-optical channel can also be used in precision measurements of the distribution of the particle momenta.

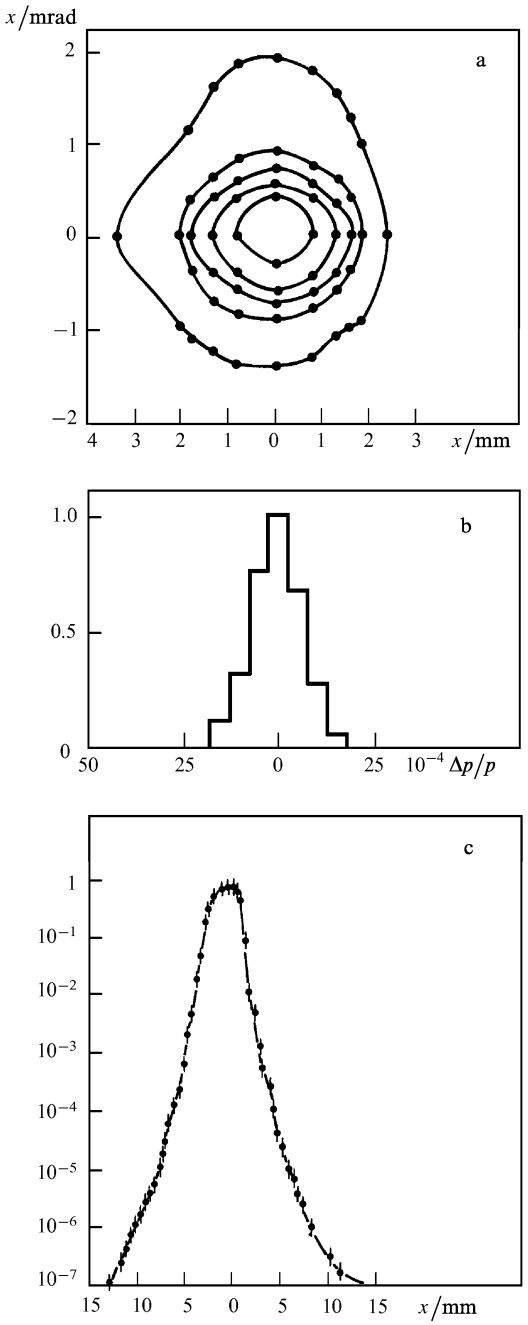

Figure 21. (a) Family of closed curves corresponding to the following phase densities of the particles (all relative to the maximum value): (*1*) 0.75; (*2*) 0.5; (*3*) 0.25; (*4*) 0.1; (*5*) 0.01. (b) Relative distribution of the particle momenta in a beam. (c) Beam profile $\rho(x,0)=N(x)$, measured by horizontal displacement of a crystal.

The coordinate x of any particle (considered ignoring the chromatic aberrations) at a detector D located at the position of the image of a crystal-deflected beam (Fig. 20) is

$$X = q_{11}X_0 + q_{13}\frac{\Delta p}{p}\,, \tag{31}$$

where q_{11} is the linear magnification coefficient; q_{13} is the linear dispersion; $X_0 \leqslant H/2$ is the initial coordinate of a particle emerging from the crystal; $\Delta p/p$ is the relative spread of the particle momenta.

If the first term in expression (31) is much less than the second, the size of the beam image is governed entirely by the spread of the particle momenta and its profile corresponds to the distribution of these momenta. In the specific case under consideration ($q_{11}=1/2$ and $q_{13}=25$ mm per 1% of $\Delta p/p$, $H=0.5$ mm) this condition is satisfied for $\Delta p/p \gg 5\times10^{-5}$. The image distortions contributed by the chromatic aberrations of a pair of quadrupole lenses amount to $\delta x/x < 2\times10^{-3}$ in the 'thin-lens' approximation [89], so that these distortions can be ignored.

The beam profile in the image was measured with the aid of an analogue ionisation chamber D in steps of 1.25 mm. The distribution of the particle momenta in the beam deduced from this profile is shown in Fig. 21b. The momentum spread in the beam in the course of extraction was $\sigma_{\Delta p/p}=6.4\times10^{-4}$.

This method of determination of the beam characteristics can be used to determine the parameters of high-intensity accelerator beams when particle counters cannot be employed.

Particularly promising is the feasibility of measuring in this way the halo of a circulating beam in large hadron colliders when the problem of particle losses is very severe.

5. Applications of bent crystals in beam extraction from an accelerator

5.1 System of accelerated-beam extraction and the first results

The ability to deflect particles through large angles in a bent crystal suggests that this method might be used to extract an accelerated beam from a vacuum chamber of an accelerator [62]. A bent crystal can be essentially regarded as a compact septum with a strong electric field of $\sim10^9$ V cm^{-1} (or higher) which is localised inside the crystal and decays at a distance of ~1 Å from its surface. A circulating beam can be targeted on a crystal in a vacuum chamber by the same methods that are used in the case of internal targets, such as the method of a local distortion of a closed orbit. Of the beam incident on the crystal only the part of it with angular divergence less than $\pm\theta_c$ is captured into the channelling mode and is deflected by an angle necessary for extraction from the accelerator vacuum chamber. The particles which are not trapped into the chanelling mode are lost partly at the nuclei in a crystal or by scattering through exceptionally large angles. However, a considerable fraction of the particles continues their motion in the accelerator ring and can cross the crystal repeatedly. Every time this happens, some of these particles are trapped into the channelling mode and are extracted from the accelerator, which naturally improves the extraction efficiency.

The simplest estimate of the overall (multiturn) extraction efficiency f_{ex} can be obtained on the basis of two assumptions: (a) the probability A of the trapping of a particle in the channelling mode in successive passages through a crystal is the same as in the first passage, $A_k = A_1$ for $k_1 > 1$ (in reality, this probability decreases with increase in the beam divergence caused by the scattering in the crystal); (b) the probability q of particle loss either in the crystal or at the walls of the vacuum chamber during the successive passages through the crystal is the same as in the first passage, $q_k = q_1$ for $k > 1$ (it can increase slightly because the particles reach the vacuum chamber walls as they are scattered). The value of q is

$\sim L/L_N$, i.e. it is equal to the ratio of the length of the crystal to the nuclear length (this ratio is of the order of 0.1). It follows from these assumptions that the formula for the overall extraction efficiency is [63]

$$f_{ex} = \frac{A}{A(1-q)+q} \exp\left(-\frac{L}{L_D}\right) . \quad (32)$$

The exponential factor takes into account the dechannelling of the trapped particles. Since both assumptions, (a) and (b), overestimate the efficiency, formula (32) represents the upper realistic limit. This formula describes well, for example, the results of computer simulation [66] of the extraction of a beam from the Superconducting Super Collider (SSC) (see Ref. [67]). The repeated passage also increases the angular acceptance of the crystal. The particles misoriented in the crystal for the first time experience a change in their angle because of their scattering and may return to the angular interval $\pm\theta_c$ in one of the subsequent passages. It is obvious that the acceptance is governed by the maximum scattering angle of a particle until it is lost in the crystal or on the walls of the vacuum chamber. It can be estimated in terms of the angle of multiple scattering occurring in the nuclear length L_N [63]:

$$\theta_N \approx \frac{14 \text{ MeV}}{pv}\left(\frac{L_N}{L_R}\right)^{1/2} , \quad (33)$$

where L_R is the radiation length. The quantity θ_N is independent of the length of the crystal and can be much greater than θ_c. Rigorous analysis of the extraction process should take into account many effects that perturb a beam: the trapping in the channelling mode and the dechannelling of the particles, multiple scattering in a crystal, scattering by the potential of bent atomic planes [64], the loss of particles in collisions with nuclei, the energy losses in a crystal, and the dynamics of motion of particles in a ring (betatron oscillations), noise, losses in the vacuum chamber walls, etc. [65]. These effects are mutually related and should be considered simultaneously [63].

The extraction of a proton accelerator beam by a crystal was first achieved in Dubna in 1984 [26] in the energy range 4.2–7.5 GeV. Extraction of a proton beam from the JINR synchrophasotron was performed by a silicon crystal with dimensions 11 mm, 10 mm, 0.4 mm, oriented along the (111) plane, and bent by an angle of 35 mrad. This crystal deflector was placed on a goniometer table, which made it possible to rotate it in steps of 40 μrad. The deflector was placed at fixed positions but at different distances from the centre of the accelerator vacuum chamber. The accelerated protons were targeted on the crystal by reducing the radius of the equilibrium orbit. The extraction was achieved at three values of the proton energy: 4.2, 6.0, and 7.5 GeV. The measured efficiency was $\sim 10^{-4}$, which was due to the low geometric efficiency $g \approx 0.4 \times 10 \text{ mm}^2/1570 \text{ mm}^2 \approx 2.6 \times 10^{-3}$, as well as due to the strong divergence of the incident beam ($\sim$2 mrad), compared with $\theta_c \approx 70$ μrad.

In 1989 a proton beam of 70 GeV energy was extracted from the IHEP accelerator [27]. Once again, silicon crystals with the (111) orientation were used and their dimensions were 65 mm, 15 mm, and 0.6 mm. The crystal deflector [69] had a wide angular acceptance $\Phi = \pm 5$ mrad, which made it easier to orient it, but this reduced the geometric efficiency by a factor of $\sim\sigma_\phi/\Phi$, where $\sigma_\phi \approx 0.3$ mrad is the beam

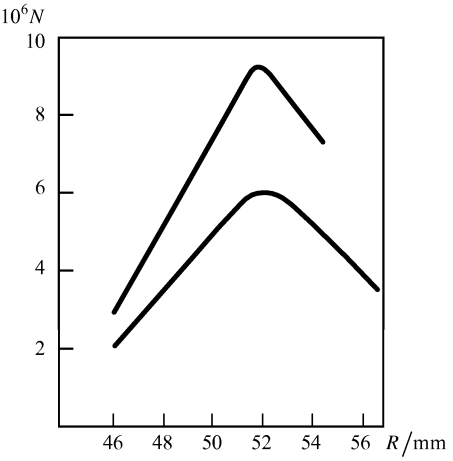

Figure 22. Dependences of the intensity of a proton beam extracted from the accelerator at the Institute of High-Energy Physics on the radial position of an internal scattering target. Beam energy (*1*) 70 GeV; (*2*) 50 GeV [28].

divergence. The crystal was bent by 85 mrad: its curvature was 1.8 mrad mm^{-1} over a distance of 30 mm and 0.8 mrad mm^{-1} over a distance of 35 mm. The crystal was placed at a distance of $\sim$ 50 mm from the equilibrium orbit. The beam was guided to the crystal by local distortion of the orbit. The efficiency achieved in this experiment was $(0.4-1.5) \times 10^{-4}$. The intensity of the extracted beam reached 4.6×10^6 protons cycle^{-1} when the intensity of the beam reaching the crystal was $\sim 10^{11}$ protons cycle^{-1}. In subsequent investigations [28] a different method for guiding the beam to the crystal was used: it involved preliminary scattering of the beam by a thin ($\sim$50 mg cm^{-2}) internal carbon target. The intensity of the beam reaching the target was $\sim 3 \times 10^{11}$ protons cycle^{-1}. Some of the scattered particles reached the crystal. The intensity of the beam extracted by this method increased to 9×10^6 protons cycle^{-1}. Calculations [28] indicated that the crystal should receive only $\sim$1/100 of the flux reaching the carbon target, so that the crystal efficiency was estimated to be 0.3%. Fig. 22 gives the dependences of the intensity of the extracted beam on the target position. In the last few years this crystal-extracted beam has been used in two experiments: PROZA and SIGMA.

5.2 Beam extraction from the Super Proton Synchrotron at CERN

The most interesting results have recently been obtained in an experiment on beam extraction by a crystal from the Super Proton Synchrotron (SPS) at CERN [29]. This experiment was designed as a comprehensive investigation of the process of extraction and, on the basis of the results obtained, for the assessment of the feasibility of beam extraction from supercolliders [74]. The experimental setup (Fig. 23) included two silicon crystals of dimensions 30 mm × 18 mm × 1.5 mm. These crystals were bent by an angle 8.5 mrad and could be used alternately for beam extraction. The beam could intersect the central (10 mm) part of a crystal avoiding a bending device of the same kind as that described in Ref. [69]. Crystals were cut parallel to a (110) plane and this orientation was accurate to within < 200 μrad. They were then polished and etched to obtain

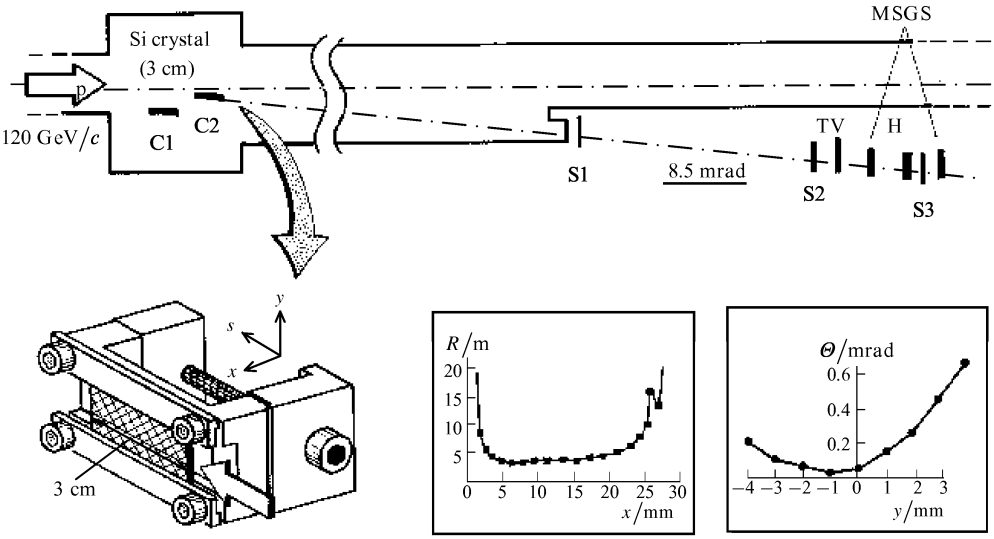

Figure 23. Crystal extraction of a beam from the Super Proton Synchrotron at CERN [29]. The bending device is shown on the left. On the right are the dependence of the crystal bending radius on the crystal length and thedependence of the orientation of the (110) planes on the vertical coordinate on the end face of a crystal.

a flat surface. A goniometer was used to orient a crystal in steps of 4 μrad and to displace it perpendicular to the beam. The protons deflected by the crystal through the angle of 8.5 mrad in the horizontal plane, towards the centre of the SPS, were detected at a distance of 20 m downstream (behind the crystal). The extracted beam was observed visually with the aid of a CsI scintillation screen (TV). The beam profiles were measured with a scintillation hodoscope (H) consisting of 32 horizontal and 32 vertical strips which were 1 mm wide. Two sets of horizontal microstrip gas chambers (MSGC), separated from one another by 1 m, were used in determination of the divergence and profile of the extracted beam. Three scintillation counters S1–S3 were used in coincidence to trigger the detectors.

Measurements were carried out on a beam of 120 GeV protons of $\sim 5 \times 10^{11}$ protons s^{-1} intensity. At this SPS energy the nonlinear effects and the natural diffusion were practically undetectable, so that the beam lifetime was > 100 hours. A crystal was placed at $\geqslant 10$ mm, corresponding to $(6-10)\sigma$ (where σ is the rms transverse beam size) from the beam axis where the halo the unperturbed beam contained practically no particles. The beam was perturbed in the horizontal plane by the electric field of a pair of capacitor plates. The capacitor field represented a white noise over a wide range and deflected particles by the rms value of ~ 0.001 μrad for every pass alongside the capacitor plates. A simulation reported in Ref. [70] indicated that protons should reach the crystal with the impact parameters (depth of penetration) of the order of 1 μm and with an angular divergence of < 5 μrad ($\theta_c = 14$ μrad). Similar impact parameters are expected in future accelerators (see Section 5.3). The structure at the edge of the crystal should therefore be of high quality.

The efficiency of the extraction process, defined as the ratio of the number of the extracted protons to the number lost in the SPS during the same time interval, was ~10%. The angular width of the intensity distribution in the extracted beam, 200 μrad (FWHM), was considerably greater than θ_c or the divergence of the incident beam. This width, as well as other observed effects (changes in the profile of the extracted beam with the misorientation of a crystal, dependence of the optimal crystal angle and of the angular width of the extracted beam on the vertical coordinate of the incident beam), were attributed to unwanted angular distortions of the end faces of the crystal resulting from the adopted bending technique (Fig. 23). All these effects were confirmed qualitatively by a simulation carried out with the aid of the CATCH program [65] which took account of the geometry of a crystal with distortions and of the effects of repeated passage of particles through a crystal. The extraction efficiency reported in Ref. [65] had a peak value ranging from 12% to 18% in the angular range 140–260 μrad (FWHM), depending on the vertical coordinate of the beam incident on the crystal and on the vertical emittance of the beam. Simulation showed that the experimental results were reproduced satisfactorily only when it was assumed that the crystal was imperfect near the surface (to a depth of ~1 μm), so that the first passage of the particles through the crystal was ineffective. The channelling and extraction of particles were possible only because of the repeated passage when the depth of penetration of the scattered particles was large. This example is also a good illustration of the main problem, which is the requirement of a high quality of the surface layer of a crystal, and of the main advantage of the use of a crystal in extraction, i.e. the feasibility of multipass transmission of particles.

The bending device was then refined to avoid the dependence of the orientation of the end face of a crystal on the vertical coordinate [30]. The angular scan width then decreased to ~70 μrad (Fig. 24), but the extraction efficiency remained as before, exactly as predicted by computer simulation [65] of beam extraction by this method. It is evident from Fig. 24 that the simulation results were in satisfactory agreement with experiments. Indirect evidence of the multipass nature of the extraction was also obtained: for example, the vertical divergence of the extracted beam was strong (this was the beam scattered during the ineffective passes through the crystal). A further

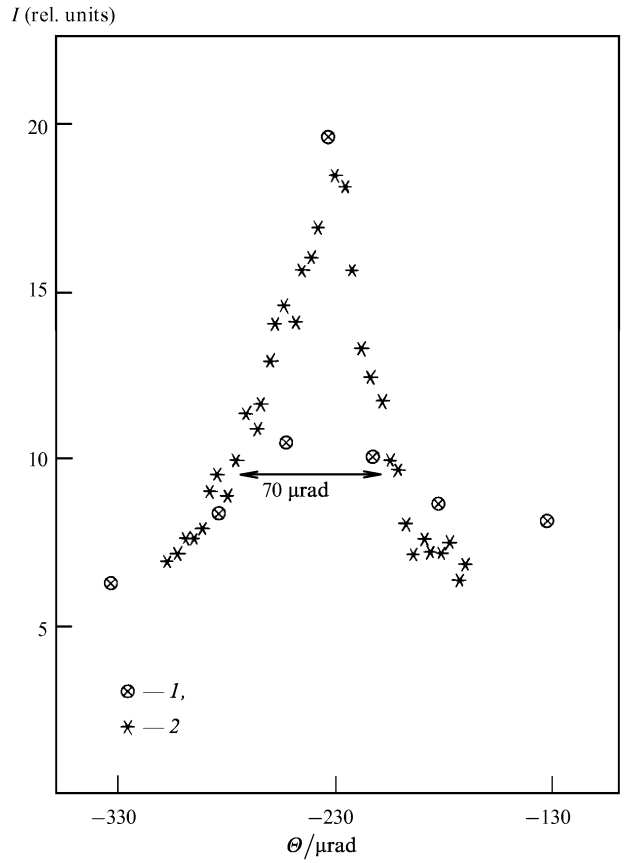

Figure 24. Dependence of the intensity of a proton beam extracted from the Super Proton Synchrotron on the angle of orientation of the crystal: (*1*) computer simulation [65]; (*2*) experimental results [30].

improvement of this extraction method will require an improvement in the crystal structure at the deflector edge. Another possibility predicted by simulation is optimisation of the contribution of repeated passages of particles by reduction of the crystal length to ~1 cm; in this case the extraction efficiency can reach ~40% even in the case of an imperfect crystal deflector [65].

5.3 Plans of beam extraction from multi-TeV accelerators

The progress in the channelling applications has stimulated interest in the possibility of beam extraction by crystals from future multiteraelectron-volt accelerators [73, 74]. In the case of the collider machines, such as the large hadron collider (LHC) under construction at CERN, a crystal provides practically the only means of extracting a beam without major losses and without significant modification of the machine. The extracted beam would be of considerable interest for the study of the beauty (B) physics experiments on a fixed target [75, 76].

The intensity of the extracted beam needed in such experiments [76] is low, $\sim 10^8$ s^{-1}, so that a crystal may be located in the halo of a circulating beam ($\sim 10^{14}$ protons in the LHC). Such a crystal can then utilise only a small part of the beam without interfering with the main experiments in the collider. The halo is formed because of the scattering of protons in the circulating beam, mainly at the beam cross points, during the operation of the collider (in the LHC the halo is $\sim 4 \times 10^9$ s^{-1}). The halo supplies a sufficient number of particles for the operation of the extraction crystal. 'Active' methods of halo formation, i.e. injection of noise into the beam, are also being studied. In view of the nonlinearity of the fields in the accelerator the halo protons diffuse slowly to the periphery and reach the crystal. The diffusion velocity is low so that the impact parameter of the first interaction of protons with the crystal is very small, $b \approx 1$ μm or even less [77]. The angular divergence of the protons incident on a crystal is also small, of the order of ± 1.5 μrad $\approx \theta_c$ for the LHC [77], which favours the use of crystals. The minimum angle of proton deflection by a crystal needed for the extraction from the LHC is only 0.7 mrad [74], so that a very high deflection efficiency should be attained.

Among the potential difficulties one can identify the following: the requirement of a high quality of the surface of a single crystal; more stringent requirements in respect of the uniformity of the orientation of the crystal face, and particularly of its edge (angular distortions amounting to $\geqslant 1$ μrad are sufficient to influence significantly the efficiency of a crystal); the requirement of a high degree of perfection of a crystal lattice (absence of dislocations). Separate problems are formation of the halo and its diffusion to the beam periphery. Both processes depend strongly on, for example, the intensity of the circulating beam, which changes during the collider operation. The use of crystals in the LHC requires tackling not only of the extraction problems themselves, but also matching of the extraction system to the beam collimation system (in order to protect the superconducting components).

The parameters of the beam incident on a crystal are similar to those in the SPS experiments. However, there is no simple way of extrapolating the SPS results to higher energies, since the multipass extraction depends on a large number of factors and these factors vary differently with increasing energy. The good agreement achieved between

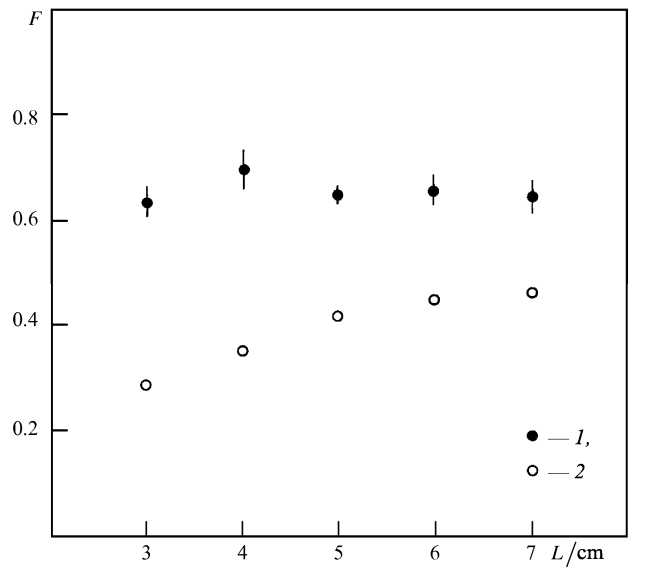

Figure 25. (*1*) Efficiency of extraction of a proton beam from the large hadron collider (LHC) by a (110) silicon crystal, plotted as a function of the crystal length. (*2*) Contribution made to the efficiency by the first passage of the particles through a perfect crystal. In each case the results are those of a computer simulation [78].

the SPS experiments and their computer simulation suggests that such simulation could also be applied to the LHC. Fig. 25 gives the dependence of the efficiency of beam extraction from the LHC on the length of a silicon crystal considered in the simulation reported in Ref. [78]. The attainable efficiency is 60% – 70% for a crystal ~5 cm long. The simulation also shows that the efficiency of beam extraction by a crystal with an imperfect 'amorphous' surface (when the extraction is entirely due to repeated incidence of the particles on the crystal) differs very little from the efficiency of an ideal crystal. This result is obtained because the particle scattering angle in a crystal is very small, of the order of the Lindhard angle, when the energy in the LHC is ~7 TeV. Investigations of beam extraction by crystals have also been carried out on the Tevatron accelerator at FNAL [72]. Computer simulations of crystal extraction of beams from other accelerators are reported in Refs [66, 79, 80].

6. Applications of bent single crystals in measurements of magnetic moments of short-lived particles

Bent crystals can be used not only in handling accelerator beams, but they also provide new opportunities for experiments in high-energy physics.

An example of such an application of a single crystal is an experiment in which the magnetic moment of the Σ^+ hyperon was measured with the aid of the FNAL accelerator [92] (the feasibility of such an experiment had been demonstrated by V M Samsonov and A V Khanzadeev [93]).

V G Baryshevskii [94] and L Pondrom [95] have shown that the magnetic moment of a particle should precess if the particle is channelled in a single bent crystal. V L Lyuboshits [96] and I J Kim [97] have developed a detailed theory of the spin precession.

The electrostatic field of the atomic planes is transformed in a bent crystal into the magnetic field in the reference frame in which the particle is at rest. The precession angle φ is therefore given by [96]

$$\varphi = \frac{1}{2}\gamma\Theta(g-2) \quad \text{for } \gamma \gg 1 ,$$

where γ is the Lorentz factor; g is the gyromagnetic ratio; Θ is the angle of deflection of a channelled particle. The measurements of φ and Θ of the channelled particle can be used to find g and, consequently, its magnetic moment

$$\mu = \frac{ge}{2mc} S ,$$

where e, m, and S are the charge, mass, and spin of the particle.

The presence of extremely strong fields in a crystal means that the magnetic moment can be determined for particles with a decay length of just a few centimetres, which is not possible to do by classical techniques in which ordinary magnets are used.

The precession of the spin of the Σ^+ hyperons was first reported in Ref. [92] and this experiment was a demonstration of the promising nature of the new method for determination of the magnetic moment of particles with heavy c- and b-quarks.

The apparatus used in this experiment included a hyperon spectrometer consisting of a dipole magnet and three arrays of strip silicon detectors, as well as a baryon spectrometer, comprising two dipole magnets and four arrays of multiwire proportional chambers.

Two bent silicon crystals (Fig. 26a) were placed behind the hyperon spectrometer at the head of the decay zone. These crystals were oriented along the (111) planes and their dimensions were $xyz = 25$ mm $\times$ 0.4 mm $\times$ 45 mm. They were bent in accordance with a three-point scheme.

The upper crystal deflected the beam downward and the lower crystal deflected it upward. The angle of the deflection was the same in both cases. Therefore, the spin precession in the crystals was in the opposite directions (black arrows in Fig. 26a).

Ionisation-loss detectors were implanted in the crystals in order to distinguish the channelled particles.

The average momentum of the Σ^+ hyperons, governed by the geometry of the hyperon channel and by the magnetic field, amounted to 375 GeV/c and the momentum scatter was $\Delta p/p = 7\%$. The measured polarisation of the Σ^+ beam was 12% $\pm$1%. At 10 m from the target the beam contained ~ 1% of the Σ^+ hyperons; the other particles were pions and protons.

The vertical dimension of the beam at the positions of the crystals was 1.8 cm and the angular divergence of the beam was 1.4 mrad. Only a small fraction of the beam, $\sim 2.5 \times 10^{-4}$, was trapped into the channelling mode (this value agreed with the calculations).

The channelled particles were identified by the angle of deflection θ and by the relatively low ionisation losses ΔE in the crystals.

The angle of deflection of the particles in the upper and lower crystals was $\theta = -1.649 \pm 0.030$ mrad and

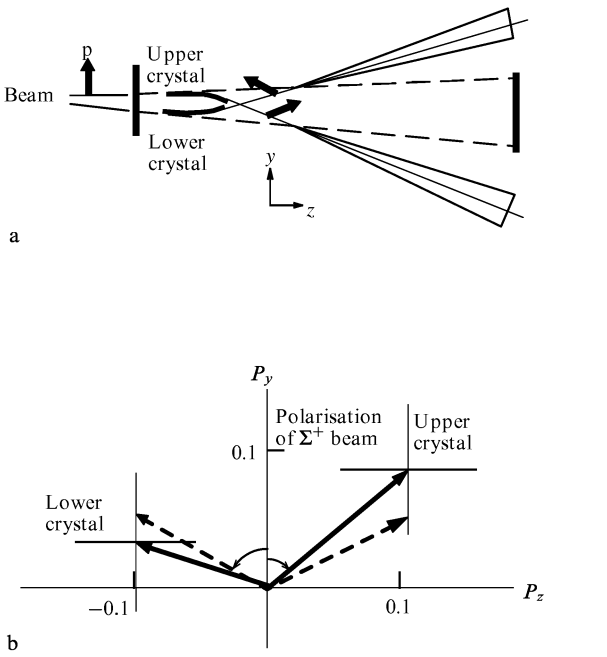

Figure 26. (a) Schematic diagram explaining the spin precession effect in a crystal. (b) Measured polarisations after the spin rotation in crystals (statistical errors are shown at the level of σ). The dashed arrows correspond to theoretical predictions.

1.649 ± 0.043 mrad, respectively (the magnetic moment should precess by $\varphi \approx 1$ rad).

The Σ^+ hyperons with the $\Sigma^+ \to p\pi^0$ decay ($\sim 52\%$ of the total number of decays) were selected for the polarisation measurements. The decay vertex was measured in a 10 m decay zone to within 50 cm. The number of events which were selected amounted to 2167 ± 47 when the event selection criterion was based on constraints imposed on the kinematic variables.

The $\Sigma^+ \to p\pi^0$ decay mode has a large asymmetry parameter $\alpha = -0.98$ and is therefore a sensitive criterion of the polarisation state of Σ^+. The components of the polarisation vector of the Σ^+ hyperons were determined for each of the crystals. They are plotted alongside the calculated data in Fig. 26b. The measured spin precession angles were $+51^\circ \pm 23^\circ$ and $-72^\circ \pm 26^\circ$ for the upper and lower crystals, respectively. The average spin precession for the two crystals, $60^\circ \pm 17^\circ$, was in agreement with the predicted value $62^\circ \pm 2^\circ$.

The average polarisation vector for the two crystals was $P = 11.8\% \pm 3.6\%$, which should be compared with the polarisation $12\% \pm 1\%$ measured without deflection in the crystals. Hence there was no depolarisation in the course of the channelling.

The measured magnetic moment of the Σ^+ hyperons was $(2.15 \pm 0.61)\mu_N$ and $(2.74 \pm 0.71)\mu_N$ for the upper and lower crystals, respectively ($\mu_N = eh/m_p$ is the nuclear magneton). The average moment $\mu = (2.40 \pm 0.46)\mu_N$ was in agreement with the published fundamental constant $(2.42 \pm 0.05)\mu_N$. The systematic error in these measurements did not exceed $0.40\mu_N$.

The experiment demonstrated the spin precession of the channelled particles in a bent single crystal. It is proposed to use this method to measure the magnetic moment of Λ_c^+, which is a short-lived particle created with a strong polarisation because of the large asymmetry parameter.

7. Summary

Two important points, which follow from an analysis of the results of investigations of the channelling of high-energy charged particles in crystals, should be stressed. First, the main assumptions made in the theory of channelling are in satisfactory agreement with experimental results. Computer programs of the CATCH type can be used to analyse results of experiments taking into account the conditions during these experiments. Second, investigations and developments in the application of bent crystals in accelerators give hope that in the near future such crystals will supplement the arsenal of means for the steering of high-energy particle beams and thus make it possible to realise certain projects which have hitherto seemed doubtful or impossible. Bent crystals are already in use in particle channels and in systems for the extraction of accelerated beams. They are opening new avenues in the design of experiments and are increasing the efficiency of the utilisation of accelerators.

This review does not deal with proposals and ideas that have not been fully developed: they are concerned mainly with the various aspects of the use of crystals in the experiments proposed for beams of particles of ultrahigh energies and are discussed in detail in Ref. [98].

Neither does this review deal with the wide range of topics related to the investigation of electromagnetic processes that occur during the passage of electrons, positrons, and high-energy γ rays through an oriented crystal. Investigations of these topics, which are opening new opportunities for the applications of oriented single crystals (in particular, the generation of polarised high-energy $e^\pm$ and γ beams in proton accelerators), have been dealt with fully during the All-Union Conference on Problems in Application of Particle Channelling Effects in Crystals to High-Energy Physics, which was held in 1991 at IHEP in Protvino, as well as in reviews [9, 10] and monographs [11–13].

References

1. Stark *J Phys. Z.* **13** 973 (1912)
2. Robinson M T, Oen O S *Phys. Rev.* **132** 2385 (1963)
3. Piercy G R, Brown F, Davies J A, McCargo M *Phys. Rev. Lett.* **10** 399 (1963)
4. Lindhard J *K. Dan. Vidensk. Selsk. Mat. Fys. Medd.* **34** (14) 64pp. (1965)
5. Gemmell D S *Rev. Mod. Phys.* **46** 129 (1974)
6. Kumakhov M A, Shirmer G *Atomnye Stolknoveniya v Kristallakh* (Atomic Collisions in Crystals) (Moscow: Atomizdat, 1980)
7. Feldman L C, Mayer J W, Picraux S T *Materials Analysis by Ion Channeling* (New York: Academic Press, 1982)
8. Ohtsuki Y H *Charged Beam Interaction with Solids* (London: Taylor and Francis, 1983)
9. Baier V N, Katkov V M, Strakhovenko V M *Usp. Fiz. Nauk* **159** 455 (1989) [*Sov. Phys. Usp.* **32** 972 (1989)]
10. Baryshevskii V G, Tikhomirov V V *Usp. Fiz. Nauk* **159** 529 (1989) [*Sov. Phys. Usp.* **32** 1013 (1989)]
11. Bazylev V A, Zhevago N K *Izluchenie Bystrykh Chastits v Veshchestve i vo Vneshnikh Polyakh* (Radiation Emitted by Fast Particles in Matter and in External Fields) (Moscow: Nauka, 1987)
12. Baier V N, et al. *Elektromagnitnye Protsessy pri Vysokikh Energiyakh v Orientirovannykh Kristallakh* (High-Energy Electromagnetic Processes in Oriented Crystals) (Novosibirsk: Nauka, 1989)
13. Akhiezer A I, Shul'ga N F *Elekrodinamika Vysokikh Energii v Veshchestve* (High-Energy Electrodynamics in Matter) (Moscow: Nauka, 1991)
14. Forster J S, Hatton H, Toone R J, et al. *Nucl. Phys. B* **318** 301 (1989)
15. Tsyganov E N, Fermilab Reports TM-682, TM-684 (Batavia, IL: Fermi National Accelerator Laboratory, 1976)
16. Elishev A F, Filatova N A, Golovatyuk V M, et al. *Phys. Lett. B* **88** 387 (1979)
17. Sun C R, Gibson W M, Kim I J, et al. *Nucl. Instrum. Methods Phys. Res. Sect. B* **230** 60 (1984)
18. Afonin A G, et al. Preprint No. 87-121 (Protvino: Institute of High-Energy Physics, 1987);
Bavizhev M D, et al. Preprint No. 87-148 (Protvino: Institute of High-Energy Physics, 1987);
Bavizhev M D, et al. Preprint No. 89-77 (Protvino: Institute of High-Energy Physics, 1989);
Galyaev N A, et al. Preprint No. 90-19 (Protvino: Institute of High-Energy Physics, 1990);
Arkhipenko A A, et al. Preprint No. 90-91 (Protvino: Institute of High-Energy Physics, 1990)
19. Andreev V A, Baublis V V, Damaskinskii E A, et al. *Pis'ma Zh. Eksp. Teor. Fiz.* **36** 340 (1982); **39** 58 (1984); **44** 101 (1986) [*JETP Lett.* **36** 415 (1982); **39** 67 (1983); **44** 129 (1986)]
20. Bak J F, Melchart G, Uggerhoj E, et al. *Phys. Lett. B* **93** 505 (1980);
Bak J F, Jensen P R, Madsboll H, et al. *Nucl. Phys. B* **242** 1 (1984)

21. Baker S I, Carrigan R A Jr, Crawford C, et al. *Phys. Lett. B* **137** 129 (1984);
Gibson W M, Kim I J, Pisharody M, et al. *Nucl. Instrum. Methods Phys. Res. Sect. B* **230** 54 (1984);
Baker S I, Carrigan R A Jr, Schailey R, et al. *Nucl. Instrum. Methods Phys. Res. Sect. A* **234** 602 (1985);
Baker S I, Carrigan R A Jr, Dixon R L, et al. *Nucl. Instrum. Methods Phys. Res. Sect. A* **248** 301 (1986)
22. Adishchev Yu N, Anan'in P S, Vorob'ev S A, et al. *Pis'ma Zh. Tekh. Fiz.* **5** 1485 (1979) [*Sov. Tech. Phys. Lett.* **5** 627 (1979)];
Medenwaldt R, Moller S P, Sorensen A H, et al. *Phys. Lett. B* **260** 235 (1991)
23. Bel'zer L I, Bodyagin V A, Vardanyan I N, et al. *Pis'ma Zh. Eksp. Teor. Fiz.* **46** 303 (1987) [*JETP Lett.* **46** 381 (1987)]
24. Chesnokov Yu, et al. Preprint No. 91-155 (Protvino: Institute of High-Energy Physics, 1991)
25. Elsener K, et al. Contributed Paper Presented at IEEE Particle Acelerator Conference, Washington, DC, 1993 (in press)
26. Avdeichikov V V, et al. *Kratk. Soobshch. OIYaI (Dubna)* (1) 3 (1984)
27. Asseev A A, Bavizhev M D, Ludmirsky E A, et al. *Nucl. Instrum. Methods Phys. Res. Sect. A* **309** 1 (1991); Preprint No. 89-57 (Protvino: Institute of High-Energy Physics, 1989)
28. Asseev A A, Myae E A, Sokolov S V, Fedotov Yu S *Nucl. Instrum. Methods Phys. Res. Sect. A* **324** 31 (1993); Preprint No. 91-182 (Protvino: Institute of High-Energy Physics, 1991)
29. Akbari H, Altuna X, Bardin S, Bellazini R, Biryukov V, et al. *Phys. Lett. B* **313** 491 (1993)
30. *RD22 Second Status Report* Report No. DRDC/94-11 (Geneva: CERN, 1994)
31. Kudo H *Nucl. Instrum. Methods Phys. Res.* **189** 609 (1981)
32. Ellison J *Nucl. Phys.* **206** 205 (1982)
33. Kaplin V V, Vorobiev S A *Phys. Lett. A* **67** 135 (1978)
34. Beloshitsky V V, Komarov F F, Kumakhov M A *Phys. Rep.* **139** 293 (1986)
35. Taratin A M, Vorob'ev S A *Zh. Tekh. Fiz.* **55** 1598 (1985) [*Sov. Phys. Tech. Phys.* **30** 927 (1985)]
36. Beloshitskii V V, Kumakhov M A *Dokl. Akad. Nauk SSSR* **212** 846 (1973) [*Sov. Phys. Dokl.* **18** 652 (1974)]
37. Waho T *Phys. Rev. B* **14** 4830 (1976)
38. Particle Data Group *Phys. Lett. B* **239** (1990)
39. Biryukov V M, Galyaev N A, et al. Preprint No. 92-156 (Protvino: Institute of High-Energy Physics, 1992); *Nucl. Instrum. Methods Phys. Res. Sect. B* **86** 245 (1994)
40. Bavizhev M D, Biryukov V M, Gavrilov Yu G *Zh. Tekh. Fiz.* **61** (2) 136 (1991) [*Sov. Phys. Tech. Phys.* **36** 203 (1991)]; *Radiat. Eff.* **25** 139 (1993)]
41. Ohtsuki Y H, Nitta H, in *Relativistic Channeling* (Eds R A Carrigan Jr, J Ellison) (New York: Plenum Press, 1987) p. 59
42. Taratin A M, Filimonov Yu M, Vyatkin E G, et al. *Phys. Status Solidi B* **100** 273 (1980); **107** 521 (1981)
43. Bavizhev M D, Biryukov V M, Report No. SSCL-N-775 (Dallas, TX: Superconducting Super Collider Laboratory, 1991)
44. Bavizhev M D, Biryukov V M, Gavrilov Yu G, Preprint No. 89-222 (Protvino: Institute of High-Energy Physics, 1989)
45. Forster J S, in *Relativistic Channeling* (Eds R A Carrigan Jr, J Ellison) (New York: Plenum Press, 1987) p. 39
46. Dearnaley G, Freeman J H, Gard G A, Wilkins M A *Can. J. Phys.* **46** 587 (1968);
Markus A M, Geguzin Ya E, Fainshtein A L *Zh. Eksp. Teor. Fiz.* **61** 332 (1971) [*Sov. Phys. JETP* **34** 621 (1972)]
47. Biryukov V M, Chesnokov Yu A, et al. *Nucl. Instrum. Methods Phys. Res. Sect. B* **73** 153 (1973)
48. Galyaev N A, et al. Preprint No. 90-147 (Protvino: Institute of High-Energy Physics, 1990);
Chesnokov Yu A, Galyaev N A, Kotov V I, et al. *Nucl. Instrum. Methods Phys. Res. Sect. B* **69** 247 (1992)
49. Kudryashov N A, Petrovskii S V, Strikhanov M N *Yad. Fiz.* **48** 666 (1988) [*Sov. J. Nucl. Phys.* **48** 426 (1988)]; *Zh. Tekh. Fiz.* **59** (4) 68 (1989) [*Sov. Phys. Tech. Phys.* **34** 422 (1989)]
50. Mannami M, Kimura K, Susuki Y, et al. *Nucl. Instrum. Methods Phys. Res. Sect. B* **33** 62 (1988)
51. Biryukov V M, in *Proceedings of Fourth All-Union Conference on Interaction of Radiation with Solids, Moscow, 1990* p. 171; *Radiat. Eff.* **25** 143 (1993)
52. Taratin A M, Tsyganov E N, Vorobiev S A *Phys. Lett. A* **72** 145 (1979)
53. Moller S P, et al. Report No. SL 93-32 (EA) (Geneva: CERN, 1993);
Moller S P, Worm T, Clement M, et al. *Nucl. Instrum. Methods Phys. Res. Sect. B* **84** 434 (1994)
54. Biryukov V M *CATCH 1.4 User's Guide* [SL/Note 93-74 (AP)] (Geneva: CERN, 1993)
55. Moller S P, Uggerhoj E, Atherton H W, et al. *Phys. Lett. B* **256** 91 (1991)
56. Jensen B N, Moller S P, Uggerhoj E, et al. *Nucl. Instrum. Methods Phys. Res. Sect. B* **71** 155 (1992)
57. Biryukov V M *Phys. Rev. E* **51** (4) (1995), in press
58. Taratin A M, Vorobiev S A *Nucl. Instrum. Methods Phys. Res. Sect. B* **47** 247 (1990)
59. Biryukov V M, Carboni G, Costantini F *Status Report on H8 Analysis* (RD22 experiment) (Pisa: Istituto Nazionale di Fisica Nucleare, 1992)
60. Biryukov V M, Bavizhev M D, Tsyganov E N, Report No. SSCL-N-777 (Dallas, TX: Superconducting Super Collider Laboratory, 1991)
61. Quere Y *Phys. Status Solidi* **30** 713 (1968)
62. Koshkarev D G, Preprint No. 30 (Moscow: Institute of Theoretical and Experimental Physics, 1977)
63. Biryukov V M *Nucl. Instrum. Methods Phys. Res. Sect. B* **53** 202 (1991)
64. Taratin A M, Vorobiev S A *Phys. Lett. A* **119** 425 (1987)
65. Biryukov V M *SL/Note 93-78 (AP)* (Geneva: CERN, 1993)
66. Shih H-J, Taratin A M, Report No. SSCL-389 (Dallas, TX: Superconducting Super Collider Laboratory, 1991)
67. Bavizhev M D, Biryukov V M, Drozhdin A I, et al. *Conference Record of the IEEE Particle Accelerator Conference, San Francisco, 1991* (New York: Institute of Electrical and Electronics Engineers, 1991) p. 177
68. Kolomenskii A A, Lebedev A N *Teoriya Tsiklicheskikh Uskoritelei* (Theory of Cyclic Accelerators) (Moscow: Nauka, 1963)
69. Bavizhev M D, Dzyba A R, Preprint No. 89-76 (Protvino: Institute of High-Energy Physics, 1989)
70. Herr W, Report No. SL/92-53 (AP) (Geneva: CERN, 1992)
71. Jensen B N, et al. ''A proposal to test beam extraction by Crystal Channeling at the SPS: a first step towards a LHC extracted beam'' Report DRDC/P29 (Geneva: CERN, 1991)
72. Carrigan R A Jr, et al. ''Proposal for a test of low intensity extraction from the Tevatron using channeling in a bent crystal'' (FNAL Proposal P853) (Batavia, IL: Fermi National Accelerator Laboratory, 1991)
73. Cox B, et al. *Proceedings of Summer Study on High Energy Physics in the 1990's, Snowmass, CO, 1988* p. 536
74. Scandale W *Proceedings of European Committee for Future Accelerators: Large Hadron Collider Workshop, Aachen, 1990* Report No. 90-20 (Geneva: CERN: 1990) Vol. 3, p. 760
75. SFT Collaboration ''An expression of interest in a super fixed target beauty facility at the SSC'' Report EOI-14 (May 1990)
76. LHB Collaboration ''Expression of interest'', in *Proceedings of General Meeting on LHC Physics and Detectors* (Geneva: CERN, 1992)
77. *The LHC Pink Book* Report No. 91-03 (Geneva: CERN, 1991)
78. Biryukov V M, Vita P F ''Simulation of an LHC beam bending with silicon crystal'' INFN-Pisa Note (Pisa: Istituto Nazionale di Fisica Nucleare, 1992);
Biryukov V *Phys. Rev. Lett.* **74** (1995), in press
79. Taratin A M, Vorobiev S A, Bavizhev M D, Yazynin I A *Nucl. Instrum. Methods Phys. Res. Sect. B* **58** 103 (1991)
80. Biryukov V M, Bavizhev M D, Tsyganov E N, Report No. SSCL-N-776 (Dallas, TX: Superconducting Super Collider Laboratory, 1991)
81. Sumbaev O I *Kristall-Difraktsionnye Gamma-Spektrometry* (Crystal-Diffraction Gamma Spectrometers) (Moscow: Gosatomizdat, 1963)

82. Samsonov V M, Preprint No. 278 (Leningrad: Institute of Nuclear Physics, 1976)
83. Bavizhev M D, Biryukov V M, Preprint No. 90-184 (Protvino: Institute of High-Energy Physics, 1990)
84. Chesnokov Yu A, et al. *Proceedings of Fifteenth International Conference on High Energy Accelerators, Hamburg, 1992* Vol. 1, p. 173
85. Andreev V A, Baublis V V, Bondar' N F, et al. *Pis'ma Zh. Eksp. Teor. Fiz.* **41** 408 (1985) [*JETP Lett.* **41** 500 (1985)]
86. Denisov A S, Fedin O L, Gordeeva M A, et al. *Nucl. Instrum. Methods Phys. Res. Sect. B.* **69** 382 (1992)
87. Kotov V I, et al. *Proceedings of Fifteenth International Conference on High Energy Accelerators, Hamburg, 1992* Vol. 1, p. 128
88. Clement M, et al. Report No. SL 92-21 (EA) (Geneva: CERN, 1992)
89. Kartashev V P, Kotov V I *Osnovy Magnitnoi Optiki Puchkov Zaryazhennykh Chastits Vysokikh Energii* (Principles of Magnet Optics of Charged High-Energy Particle Beams) (Moscow: Energoatomizdat, 1984)
90. Jensen B N, et al. Report No. SL 92-14 (EA) (Geneva: CERN, 1992)
91. Chesnokov Yu A, Dudenko V V, Galyaev N A, et al. *Nucl. Instrum. Methods Phys. Res. Sect. B* **63** 366 (1992)
92. Chen D, Albuquerque I F, Baublis V V, et al. *Phys. Rev. Lett.* **69** 3286 (1992)
93. Samsonov V M, Khanzadeev A V, Preprint No. 1476 (Leningrad: Institute of Nuclear Physics, 1987)
94. Baryshevskii V G *Pis'ma Zh. Tekh. Fiz.* **5** 182 (1979) [*Sov. Tech. Phys. Lett.* **5** 73 (1979)]
95. Pondrom L *Proceedings of 1982 Summer School on Elementary Particle Physics and Future Facilities, Snowmass, CO* (Ed. R Donaldson) (Batavia, IL: Fermi National Accelerator Laboratory, 1983)
96. Lyuboshits V L *Yad. Fiz.* **31** 986 (1980) [*Sov. J. Nucl. Phys.* **31** 509 (1980)]
97. Kim I J *Nucl. Phys. B* **229** 251 (1983)
98. Sun C R, in *Relativistic Channeling* (Eds R A Carrigan Jr, J Ellison) (New York: Plenum, 1987) p. 379